Green Chemistry

ROYAL SOCIETY OF CHEMISTRY

CRITICAL REVIEW

View Article Online
View Journal | View Issue

Cite this: *Green Chem.*, 2024, **26**, 1041

Challenges and opportunities for the photo-(thermal) synthesis of ammonia

Diego Mateo,* Angel Sousa, Maksim Zakharzhevskii and Jorge Gascon *

For more than one century, the synthesis of ammonia (NH_3) through the Haber–Bosch route has allowed the industrial-scale production of fertilizers and other nitrogen-containing compounds. Despite its success, the development of alternative NH_3 synthesis methods with a lower CO_2 footprint is highly desirable. In this context, the use of sunlight as source of energy to perform the photo-catalytic nitrogen (N_2) reduction reaction represents a promising approach, although the reported efficiencies remain below those required to compete with the traditional HB route. To overcome these limitations, photo-thermal catalysis offers the opportunity to synergistically combine the effect of photo-induced charge carriers and localized heat to perform the synthesis of ammonia. In this review, we first provide an overview of the most recent advances in thermo- and photo-catalytic NH_3 production. Next, we describe the merits of photo-thermal catalysis to enhance the catalytic activity towards NH_3 synthesis. To conclude, we share our viewpoint on the future prospects and challenges ahead for photo-thermal catalysis to become a reality in the production of NH_3 and other industrially relevant chemicals.

Received 10th August 2023,
Accepted 6th December 2023

DOI: 10.1039/d3gc02996d

rsc.li/greenchem

Introduction

Ammonia (NH_3) synthesis is considered one of the most relevant processes in the chemical industry. Together at BASF, German chemists Fritz Haber (1868–1934) and Carl Bosch (1874–1940) developed in 1913 the so-called Haber–Bosch (HB) process for the industrial-scale manufacturing of ammonia.[1,2] This breakthrough contributed to the extensive production of NH_3 and its application to the large-scale fabrication of fertilizers, explosives and other nitrogen-containing chemicals of industrial interest. After more than one century, the actual ammonia synthesis has barely changed, and indeed *circa* 95% of the total ammonia production is still obtained through the Haber–Bosch route.

Despite the success of the traditional thermo-catalytic ammonia synthesis, the pursuit of higher efficiency, cost reduction, and environmental sustainability remains ongoing. In this regard, the synthesis of ammonia consumes 3–5% of the world's natural gas production, representing 1–2% of the annual energy supply and approximately 1% of all greenhouse gas generation.[3,4] In view of this, the current focus of research aims to further optimize the process and explore novel approaches to meet the rising global demand for ammonia while minimizing energy consumption and greenhouse gas emissions. One promising strategy in this vein is the use of blue hydrogen (H_2) for ammonia production.[5] This method leverages existing fossil fuel infrastructure for exploitation and distribution while minimizing carbon dioxide (CO_2) emissions through carbon capture and storage (CCS). Recent reports indicate, indeed, that the use of blue ammonia can be a present-day convenient solution to mitigate the climate impacts associated with the conventional ammonia production route, at least until green ammonia becomes economically profitable.[6] In fact, in September 2020 ARAMCO and the Institute of Energy Economics (Japan), in partnership with SABIC, successfully achieved the production and shipment of blue ammonia from Saudi Arabia to Japan, thus representing the world's first blue ammonia supply-chain demonstration.[7] Unfortunately, this approach still relies on fossil gas, leading to a high concentration of HB facilities near the gas supply points and increasing transportation costs to remote or underdeveloped locations.[8]

To achieve decentralized ammonia production and move towards a carbon-free economy, alternative methods for the reduction of nitrogen (N_2) have been proposed. Among these methods, photo-catalysis represents an intelligent approach to drive chemical reactions by taking advantage of the solar energy. Assuming water or renewable H_2 as source of protons, photo-catalysis enables a CO_2-free NH_3 synthesis using sunlight as driving force. Besides, this strategy offers the additional advantage of allowing small on-site NH_3 synthesis plants powered by renewable energy, which essentially favors local production of ammonia close to the final consumption

Advanced Catalytic Materials, KAUST Catalysis Center (KCC), King Abdullah University of Science and Technology (KAUST), Thuwal 23955, Saudi Arabia. E-mail: Jorge.gascon@kaust.edu.sa, Diego.mateo@kaust.edu.sa

points. Nevertheless, and despite all these potential benefits, the reported efficiencies of most of the photo-catalytic systems for N_2 fixation described to date are still insufficient to meet industrial-scale requirements.[9]

In this context, the integration of both thermo-catalysis and photo-catalysis (from now on, "photo-thermal catalysis") has lately appeared as an excellent opportunity to both reduce the energy requirements and increase the catalytic efficiency of many chemical processes, including CO_2 conversion, H_2 generation or the degradation of pollutants, among others.[10–15] Thanks to the combination of photo-induced localized heating and photo-excited charge carriers, many photo-thermal catalysts have exhibited comparable or even higher catalytic rates than those displayed under pure thermal conditions. For these reasons, it is quite surprising that, to date, only a few works have drawn attention to the synergistic combination of light and heat to perform the NH_3 synthesis reaction, thus remaining as an almost unexplored field of research. Given the emerging prospects of photo-thermal catalysis and the extraordinary relevance of ammonia in our modern societies, we herein present a review of the newest advances in thermo-catalytic, photo-catalytic and synergistic photo-thermo-catalytic NH_3 synthesis during the last five years. The goal is to give an overview of the up-to-date strategies of traditional thermo- and photo-catalytic NH_3 production and, at the same time, to highlight the potential of photo-thermal catalysis as a hybrid tool to break the limitations of its individual thermochemical and photochemical counterparts. In this review, we will first briefly introduce the most well-accepted reaction pathways for NH_3 synthesis in thermo- and photo-catalysis. Then, we will describe recent advancements in thermo-catalytic and photo-catalytic NH_3 synthesis, paying special attention to novel strategies to moderate reaction conditions and/or improve the catalytic performance. After that, we will outline a summary of the merits of photo-thermal catalysis to boost the catalytic activity towards NH_3 production, giving specific examples found in the literature. Lastly, we will share our opinion on the future directions and challenges ahead for photo-thermal catalysis to become a viable technology for the production of NH_3 and other commodities of industrial interest.

Reaction pathways for NH_3 synthesis

The reaction of N_2 and H_2 to produce NH_3 (eqn (1)) is an exothermic process thermodynamically favored by high pressures and low temperatures.

$$N_2 + 3H_2 \leftrightarrow 2NH_3 \quad \Delta H^\circ = -92.2 \text{ kJ mol}^{-1} \qquad (1)$$

Mechanistically, the catalytic N_2 reduction reaction is a multi-step process that involves: (i) N_2 adsorption, (ii) N≡N bond activation and/or cleavage, (iii) $N_{2(ads)}$ or $N_{(ads)}$ hydrogenation and (iv) NH_3 desorption.[16,17] Traditionally, two broadly accepted mechanisms have been proposed for the N_2 reduction reaction, namely the dissociative pathway and the associative pathway (Fig. 1).[18]

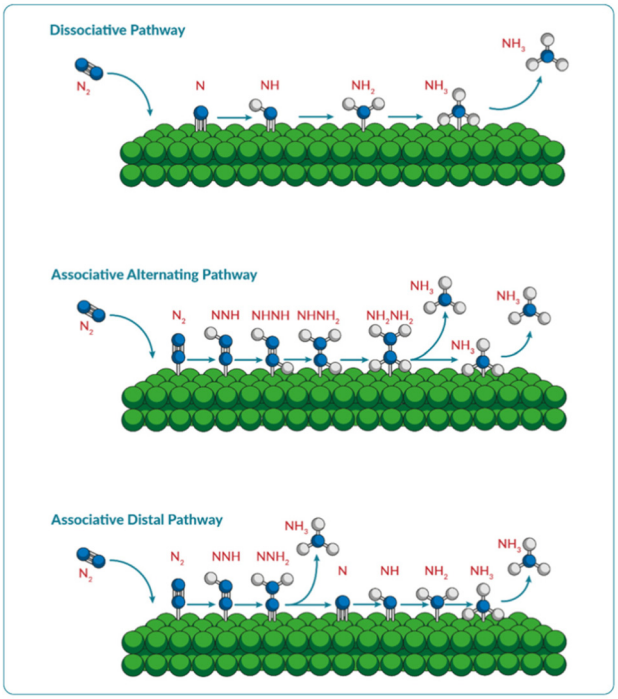

Fig. 1 Reaction pathways for the N_2 reduction reaction to ammonia. Adapted with permission from ref. 18. Copyright (2017) Elsevier.

In the dissociative pathway, the N≡N bond cleavage takes place before the hydrogenation of the nitrogen atom. In view of the high dissociation energy of the first N–N bond (410 kJ mol^{-1}), this route is extremely energy-intensive, and, indeed, traditional thermochemical HB systems are believed to follow this mechanism for the production of ammonia.[19] On the contrary, the associative pathway is based on the sequential hydrogenation of nitrogen atoms while bonded to each other. Two different sub-types of associative pathways are possible depending on the hydrogenation site.

In the alternating associative pathway, nitrogen atoms of adsorbed N_2 are successively hydrogenated and, eventually, NH_3 is desorbed after the cleavage of the N–N bond. In the distal associative pathway, however, the hydrogenation occurs preferably on the distal nitrogen atom.[9] Overall, the associative pathway does not require the cleavage of the first bond in N_2 molecule so in these cases the energy requisites are considerably lower. In consequence, the associative pathway is expected to be the preferential mechanism for electro- or photo-catalytic NH_3 production systems.

Thermo-catalytic NH_3 synthesis

As previously mentioned, NH_3 synthesis reaction is thermodynamically enhanced at high pressures and low temperatures. From a kinetic point of view, however, temperatures above 200 °C are necessary in order to achieve significant conversion values. For these reasons, as a compromise between kinetics

and thermodynamics, thermo-catalytic NH_3 synthesis is generally conducted under medium temperatures and high pressures (400–450 °C and 150–250 atm), achieving conversion rates of 10–15% per pass.[20] These operating conditions represent the main drawback for the thermo-catalytic NH_3 synthesis, not only for the elevated consumption of energy but also for the limited stability of the catalysts. For these reasons, one of the main challenges in the field is the development of systems which enable milder reaction conditions, especially in terms of operating pressure, as compression cycles represent the major capital cost of the whole HB process.

Fe-based catalysts

Iron-based catalysts represent, undoubtedly, the most investigated and applied materials in the NH_3 synthesis reaction. Particularly, iron-fused catalyst derived from hematite (Fe_2O_3), magnetite (Fe_3O_4) and/or wüstite ($Fe_{1-x}O$) are the most commonly used in modern industries. Nevertheless, it is also true that early studies conducted with iron catalysts at BASF facilities showed quite disappointing activities and, in fact, this served as a spur for the study of the effect of additives on the catalytic performance. A comprehensive investigation was developed in between 1909 and 1911 by Carl Bosch's assistant Alwin Mittasch, who conducted a systematic testing of 2500 different materials in order to find an efficient and stable catalyst for the NH_3 synthesis.[21] The scrutiny was prolonged until 1922 including about 5000 different candidates and eventually the best catalyst resulted to be a multi-component mixture consisting of magnetite-based iron catalyst with small amounts of alumina, calcium oxide, and potassium alkali.[21] This exhaustive screening demonstrated the importance of the addition of promoters to the formulation of catalysts in order to provide beneficial structural and electronic effects, as we will later elaborate in this review.

Supported iron catalysts are also an appealing subfamily of ammonia synthesis catalysts. In these cases, carbon or metal oxides usually act as support materials for active iron species. When it comes to carbon-based catalysts, the one-step pyrolysis of metal–organic compounds has lately emerged as a straightforward method to obtain well-dispersed metal nanoparticles (NPs) encapsulated into a carbon matrix. For instance, Morlanés *et al.* developed a novel catalyst based on iron NPs embedded on carbon through the controlled pyrolysis at 735 °C of iron phthalocyanines.[22] Upon promotion with Cs, the as-prepared catalyst (10%Cs-FePc) exhibited a stable production of NH_3 in the order of 14 000 μmol g^{-1} h^{-1} at 400 °C and 3 MPa, even surpassing an iron benchmark catalyst (Fe_KM1) under similar reaction conditions (Fig. 2A–C). Long-

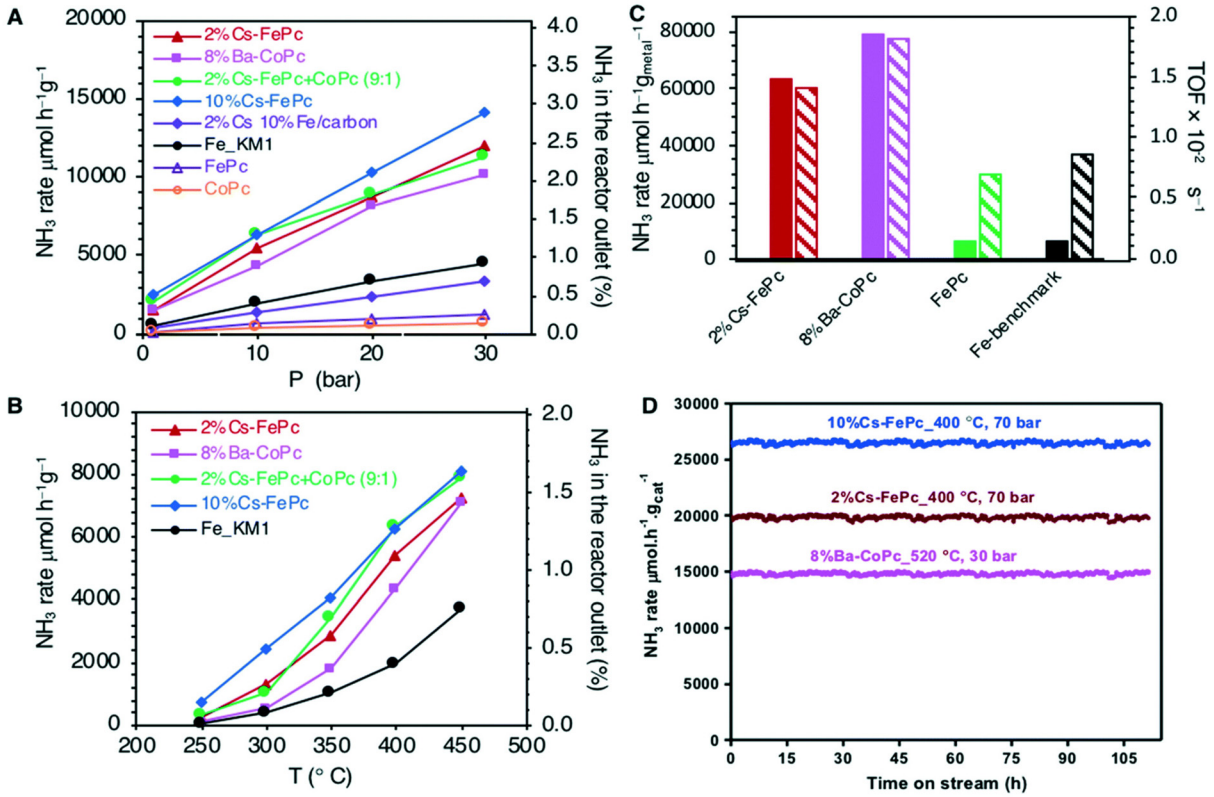

Fig. 2 Catalytic performance of the phthalocyanine-derived catalysts for the ammonia synthesis reaction. (A) Pressure effect on the NH_3 synthesis rate at 400 °C. (B) Temperature effect on the NH_3 synthesis rate at 1 MPa. (C) Specific activity in μmol NH_3 h^{-1} g_{metal}^{-1} and TOF (s^{-1}) (diagonal stripes) at 400 °C and 3 MPa. (D) Stability tests in the range of 400–520 °C and 3–7 MPa. Reproduced with permission from ref. 22. Copyright (2020) Royal Society of Chemistry.

term stability tests also demonstrated an outstanding stability of the catalyst after more than 100 hours of reaction (Fig. 2D).

The promotion with Cs was crucial to boost the catalytic activity and authors speculated that the presence of alkali both decreased the energetic barrier for nitrogen dissociation and increased the number of surface active sites by destabilization of adsorbed NH_x species. Interestingly, homologous materials prepared by conventional impregnation of carbon with iron/alkali displayed much lower activity. The authors concluded, therefore, that the remarkable stability and catalytic activity of 10%Cs-FePc directly stemmed from the synthetic approach based on the pyrolysis of phthalocyanine precursor. A follow-up work from the same group demonstrated that it was also possible to obtain highly efficient bimetallic Fe–Co catalysts through the physical mixture of Fe and Co phthalocyanines followed by the pyrolysis treatment.[23] Under the optimal Fe : Co ratio, the bimetallic catalyst outperformed the monometallic Fe and Co counterparts, exhibiting a NH_3 production of 53 666 μmol g^{-1} h^{-1} at 400 °C and 7 MPa. In a related precedent, the groups of Zou and Ma reported a K-promoted Fe/C catalyst derived from the pyrolysis under He of Fe-based metal–organic-framework (MOF) xerogels.[24] Upon addition of 1% K to the MOF-derived Fe catalyst, the catalytic activity reached 30 400 μmol g^{-1} h^{-1} at 400 °C and 3 MPa, approximately 3 times higher compared to the sample without potassium. X-ray photoelectron spectroscopy (XPS) measurements revealed a shift to lower binding energies for the Fe 2p peak along with the increase of potassium concentration in the samples, thus suggesting a charge transfer from K ions to the surface of iron. Eventually, this electron-rich environment on the Fe surface favors nitrogen activation and improves the catalytic activity of promoted samples. Curiously, potassium not only enhanced the catalytic performance by modulating the electronic properties of the Fe active sites but also by increasing the thermal stability of the catalyst. Authors observed that unpromoted samples suffered from a severe deactivation after 24 h of reaction under high temperature conditions (475 °C). *In situ* temperature-programed reaction-mass spectrometry (TPR-MS) measurements demonstrated that the deactivation of the samples stemmed from the methanation of the catalyst under reaction conditions, which at the end led to carbon loss and agglomeration of Fe nanoparticles. However, under the same reaction conditions K-promoted samples retained more than 90% of their activity due to the inhibition of the methanation reaction by potassium.

Apart from carbon, oxyhydrides have been recently explored as potential supports in the formulation of new NH_3 synthesis catalysts. In these cases, a low content of iron in the order of 1–2% in weight is deposited on the inorganic support, in sharp contrast with the high iron loading of up to 50% that can be achieved through the controlled pyrolysis of Fe-containing carbon-based precursors. For example, the groups of Kobayashi and Kageyama reported the preparation of 1% Fe/$BaTiO_{2.35}H_{0.65}$ catalyst with a remarkable catalytic activity of 14 000 μmol g^{-1} h^{-1} at 400 °C and 5 MPa.[25] Authors found that the oxyhydride support could successfully inhibit H_2 poisoning by removing the excess of adsorbed hydrogen through an effective spillover pathway. Furthermore, the oxyhydride served as electron donation source to the Fe metal sites, thus reducing the strength of the triple bond of adsorbed N_2 and, consequently, improving the catalytic activity. Further research from Kitano and co-workers demonstrated that the presence of other heteroanions like nitride (N^{3-}) could enhance even more the performance of oxyhydrides as NH_3 catalysts.[26] In this regard, authors developed a new perovskite oxynitride–hydride $BaCeO_{3-x}N_yH_z$ loaded with small amounts of Fe (1.2 wt%). Using this catalyst, the NH_3 synthesis rate at 400 °C and 0.9 MPa was 6800 μmol g^{-1} h^{-1}. In comparison, Fe-supported $BaCeO_3$ displayed a catalytic rate in the range of 30 μmol g^{-1} h^{-1}. Authors performed additional isotopic experiments in order to disentangle the promotion effect of Fe-$BaCeO_{3-x}N_yH_z$ and found that, unexpectedly, the rate-determining step shifted from N_2 dissociation to N–H bond formation due to the presence of N^{3-} and H^- anions. Ultimately, this change in the reaction mechanism translated into a lower activation energy for the ammonia synthesis (46–62 kJ mol^{-1}). In the case of Fe-$BaCeO_3$, however, the NH_3 formation followed the conventional mechanism characterized by high-energy barriers (85–121 kJ mol^{-1}).

Ru-based catalysts

In spite that iron-based catalysts have enjoyed a historical hegemony in the Haber–Bosch process, it was in the 1970s when a consortium between British Petroleum and M.W. Kellogg companies developed a novel carbon-supported ruthenium catalyst (Ru/C) for the NH_3 synthesis reaction.[27] Since then, the research on innovative Ru-based catalysts has gained considerable relevance and a vast number of supports such as perovskites, oxides or carbon-derived materials have been investigated.[28–33]

For instance, the use of ceria (CeO_2) has been extensively reported due to its abundant oxygen vacancies that increase the electron density of Ru sites to promote N_2 activation.[34] Furthermore, it has been found that parameters like morphology of CeO_2 or metal–support interaction are key to maximize the catalytic activity of the resultant materials.[35] In this regard, Ma and co-workers compared the catalytic activity for NH_3 synthesis of three different morphologies of ceria (nanocubes, nanorods, and nanoparticles) with a nominal Ru loading of 4%.[36] At 400 °C and only 1 MPa, ceria nanorods displayed the highest catalytic activity (3830 μmol g^{-1} h^{-1}) followed by ceria nanocubes (1289 μmol g^{-1} h^{-1}) and ceria nanoparticles (529 μmol g^{-1} h^{-1}). XPS measurements also revealed the presence of CeH_{2+x} hydride on the samples and, curiously, authors identified a positive correlation between the amount of this hydride and the catalytic activity. Basically, the role of the CeH_{2+x} species seemed to be the electron donation to the Ru active sites, thus increasing the catalytic performance towards NH_3 synthesis. More recently in 2021, Li and collaborators described how the treatment of Ru-CeO_2 catalyst with hydrazine (N_2H_4) could modulate the electronic metal–support interaction and boost the catalytic activity in the NH_3 synthesis

reaction.[37] Authors found that the mild reduction of Ru–CeO_2 with hydrazine followed by H_2 treatment at 500 °C caused an increase in (i) the fraction of metallic Ru, (ii) the concentration of Ce^{3+} and (iii) the number of exposed species of Ru compared to the conventional reduction with only H_2. In the absence of N_2H_4 treatment, oxygen migration from the ceria support to the Ru species led to the lowering of exposed metallic Ru. However, the treatment with N_2H_4 improved the electronic metal–support interaction to create electron-rich states at the Ru sites and, eventually, increased the activity of Ru-CeO_2. Interestingly, a very recent work from Feng and collaborators revealed that ceria could act not only as a support but also as a promoter of Ru-based catalysts.[38] In their work, authors deposited small clusters of ceria on a Ru/Al_2O_3 catalyst and demonstrated that these sub-nanometric ceria domains could prevent the H_2 poisoning of Ru active sites. Furthermore, XPS data suggested that ceria clusters acted as electron donors to modulate the electronic structure of Ru, thus facilitating the N_2 adsorption and H_2 dissociation on its surface. Apart from ceria, other metal oxides such as MgO, La_2O_3 or Y_2O_3 have been recently explored as potential supports for Ru-based catalysts for the HB reaction.[39–41]

Besides metal oxides, other materials like hydrides, nitrides, or amides have lately demonstrated to be excellent hosts for Ru in the preparation of new ammonia synthesis catalysts, even outperforming their Fe-based counterparts.[42–45] For instance, Kitano *et al.* developed a $Ru/Ca(NH_2)_2$ catalyst promoted with Ba to create Ru–Ba core–shell nanoparticles supported on the calcium amide.[45] The as-prepared catalyst displayed an outstanding activity towards NH_3 synthesis of 60 400 μmol g^{-1} h^{-1} at 360 °C and pressure as low as 0.9 MPa, thus exceeding by 6 times the performance of the industrial benchmark Fe catalyst (Fig. 3). Furthermore, Ru–Ba/$Ca(NH_2)_2$ could operate at relatively low temperatures below 300 °C, achieving NH_3 production rates of 7500 μmol g^{-1} h^{-1} at only 260 °C.

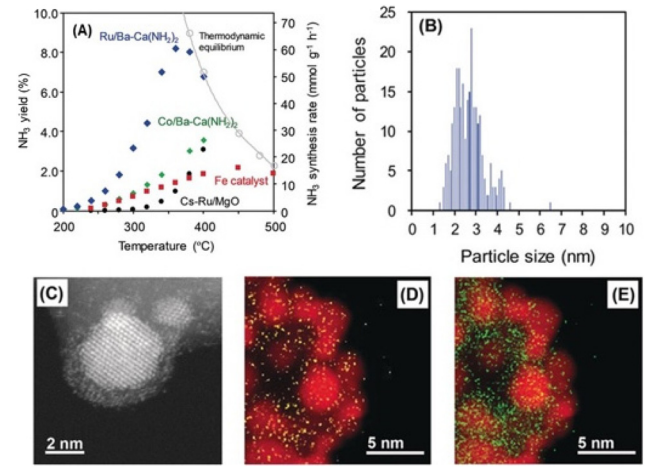

Fig. 3 (A) Temperature dependence on the catalytic performance of Ru/Ba-$Ca(NH_2)_2$ catalyst for the ammonia synthesis reaction at 0.9 MPa. (B) Particle size distribution and (C) HAADF-STEM image of Ru/Ba-Ca$(NH_2)_2$ catalyst. EDX elemental mapping images of (D) Ba (yellow) and (E) Ca (green), where Ru is displayed as red. Reproduced with permission from ref. 45. Copyright (2018) John Wiley and Sons.

In fact, one of the main advantages of Ru catalysts compared to their Fe-based equivalents lies in their improved catalytic activities under mild reaction conditions of temperature and pressure, therefore contributing to a considerable reduction of the capital cost of ammonia plants. Nevertheless, it is still hard to imagine a scenario in which Ru catalysts widely substitute traditional Fe catalysts, especially if one takes into account the high cost and limited availability of Ru. In the specific case of carbonaceous supports, the presence of Ru can also lead to the partial loss of the carbon due to its detrimental methanation, thus reducing the long-term stability of the catalyst.[46] All these drawbacks still hamper the broad implementation of Ru catalysts in conventional Haber–Bosch plants and, indeed, by 2010 only sixteen ammonia plants around the globe operated using commercial ruthenium-based catalysts.[21]

Co-based catalysts

Alternative first-raw transition metals like cobalt or nickel have been explored in recent years as potential catalysts for NH_3 synthesis.[47,48] Particularly for Co-based catalysts, notable catalytic activities at moderate operating conditions were achieved. For example, in a similar way to Fe catalysts derived from the pyrolysis of carbonaceous precursors, in 2020 Morlanés and collaborators reported the use of a barium-promoted Co/C catalyst obtained from the pyrolysis of Co phthalocyanine at 735 °C.[22] The as-prepared materials displayed an ammonia production of 10 250 μmol g^{-1} h^{-1} at 400 °C and 3 MPa. As in the case of Cs for Fe/C catalyst, the promotional effect of Ba on Co/C catalyst was uniquely ascribed to its electron donation activity but not to a protective effect against methanation of the carbon support. In 2015, the group of Pilecka evaluated the effect of barium as promoter of an activated carbon-supported Co catalyst for ammonia production.[49] Under optimal conditions, Ba–Co/C catalyst achieved a NH_3 production of 88 235 μmol g^{-1} h^{-1} at 400 °C and a high pressure of 9 MPa. However, in contradiction with the work of Morlanés *et al.*, in this case authors found that even small amounts of Ba were able to enhance the catalytic activity by suppressing the undesirable methanation of the carbon matrix. All these results suggest that the nature and preparation protocol of the carbonaceous supports are decisive to determine both the activity and stability of the resultant catalysts.

The use of inorganic supports has been also described in the formulation of Co-based catalysts. Kitano and co-workers prepared a perovskite oxynitride-hydride, $BaCeO_{3-x}N_yH_z$, which was loaded with a 4.7 wt% of Co.[26] The as-prepared catalyst achieved an outstanding NH_3 production rate of 10 100 μmol g^{-1} h^{-1} at 400 °C and a very low pressure of 0.9 MPa. When authors decreased the temperature to 300 °C keeping constant the pressure, the catalytic activity significantly decreased to ~2000 μmol g^{-1} h^{-1}. It is worth noticing that, under the same reaction conditions, an analogous cata-

lyst with a 4.3 wt% of Ru displayed a NH_3 production rate close to 5000 μmol g^{-1} h^{-1}, thus highlighting the promising attributes of Co-based catalysts. In the last years, the group of Jiang has performed an extensive research on Co/CeO_2-based catalysts for the HB process. As we discussed in the previous section for CeO_2-supported Ru catalysts, authors found that the shape of CeO_2 (polyhedral, nanorods or hexagonal morphology) was critical to optimize the catalytic performance of a series of Co-based catalysts.[50] Authors suggested that the morphology had a strong influence of the reducibility of both Co oxides and CeO_2 support, thus modifying the metal–support interaction. Co NPs supported on CeO_2 polyhedrons displayed the best catalytic activity achieving 86 000 μmol g^{-1} h^{-1} at 430 °C and 10 MPa. In a follow-up work, the same authors studied the effect of alkali promoters (Ba and K) on the catalytic activity of Co/CeO_2 catalysts.[51] Quite surprisingly, Ba showed a positive effect on the performance but the addition of K, even at small quantities, was detrimental to improve the catalytic activity. Later in 2019, authors made a last effort to strengthen the metal–support interaction of Co/CeO_2 catalysts.[52] To this end, they used dopamine during the synthesis to favor the stability of Co NPs and increase the interaction between Co and CeO_2 thanks to a strong interfacial bonding. This improved metal–support interaction was accompanied by a reduction of the particle size of Co, a better reducibility and a lower activation energy for N_2 desorption. Under optimal conditions, the Co/CeO_2 catalyst exhibited an outstanding NH_3 production rate of 19 120 μmol g^{-1} h^{-1} at 425 °C and a pressure as low as 1 MPa.

In general, most of the productivity values presented in this section are comparable or even outperform those achieved by many Ru-based catalysts. Taking into account that the main advantage of Ru-based catalysts is the possibility to operate under low pressure, Co-based catalysts have exhibited a huge potential to compete with Ru in the development of efficient yet affordable NH_3 catalysts operative under mild reaction conditions.

Photo-catalytic NH_3 synthesis

As discussed above, the traditional HB synthesis heavily relies on fossil energy sources (particularly the steam methane reformers for the production of H_2), thus contributing to estimated CO_2 emissions in the order of 1.5–1.6 tons of CO_2 per ton of NH_3.[53] For this reason, the introduction of water or renewable hydrogen (even blue hydrogen in the worst-case scenario) as reducing agents constitutes a key improvement to mitigate the carbon footprint of the NH_3 synthesis reaction. In addition to this, the implementation of renewable energy (either wind or solar) to drive the full process would further contribute to alleviate CO_2 emissions associated to the HB process.

With this in mind, photo-catalysis has emerged as a viable strategy to achieve a low-carbon emitting NH_3 synthesis route. On the one hand, photo-catalysis offers the possibility to integrate water as source of protons for the N_2 reduction reaction. On the other hand, photo-catalysis uses sunlight as unique driving force and operates under mild reaction conditions of pressure and temperature, therefore decreasing the global energy requirements of the process. Consequently, the photo-catalytic NH_3 synthesis represents a promising strategy to overcome the limitations of the conventional thermo-catalytic pathway and, indeed, over the last years it has become a very dynamic field of research.[54–57]

Despite these encouraging features, the catalytic performance of most of the photo-catalytic NH_3 synthesis systems reported to date is still insufficient to meet the requirements for any industrial scale-up of this technology. This is mainly due to the limited utilization of sunlight by many photo-catalysts, the fast recombination rate between photo-generated electrons and holes and the slow reaction dynamics characteristic of photo-catalytic processes. These shortcomings are, obviously, shared by all photo-catalytic reactions but, particularly for the nitrogen reduction reaction, the process is even more complex considering the extremely high reduction potential (−4.2 eV *vs.* NHE) necessary to activate molecular nitrogen.[19] Although it is possible to circumvent this thermodynamic limitation through alternative multiple-electron transfer processes with lower reduction potentials, this entails slower reaction kinetics that, inevitably, decrease the productivity of the photo-catalytic system. Furthermore, even if the photo-catalyst possesses a sufficiently high reduction potential at its conduction band to make the N_2 reduction thermodynamically feasible, the selectivity can be compromised due to presence of the undesirable H_2 evolution reaction under aqueous media, thus further reducing the overall efficiency of the process.

All the above-mentioned drawbacks have motivated active lines of research devoted to improve the efficiency and the selectivity of photo-induced NH_3 synthesis. Therefore, in the following sections of this review we will describe the current advances in the design of novel photo-catalysts, paying special attention to different strategies to overcome the limitations that still impede photo-catalysis from becoming a viable route for NH_3 production.

Inorganic semiconductors

TiO_2-based catalysts. Among all inorganic semiconductor oxides, titanium oxide (TiO_2) has been the most studied material in photo-catalysis for a wide variety of applications including environmental remediation, production of solar fuels and, of more relevance for the scope of this review, NH_3 synthesis. In fact, it was in 1977 when Schrauzer and Guth reported for the first time the use of a series of doped-TiO_2 for the photo-catalytic reduction of N_2 in water to produce NH_3.[58] Since then, many works have explored TiO_2-based photo-catalysts for the production of ammonia, although the reported efficiencies are still far from satisfactory.[59–62]

Defect engineering has recently gained considerable relevance as a tool to enhance the catalytic activity in semiconductor photo-catalysts. Thus, for example, the introduction of oxygen vacancies, heteroatom doping or lattice distortions can modify the surface, chemical and/or light absorption properties.[63,64] When it comes to light-induced NH_3 synthesis,

TiO_2-based catalysts have also benefited from this strategy to improve their catalytic performance. For instance, Zhang and co-workers developed ultrathin defective TiO_2 nanosheets through doping with copper ions.[65] Upon doping with Cu, authors increased the oxygen vacancy (VO) defect states and this translated into an enhancement in the light absorption in the range of 400–800 nm (Fig. 4A). These new absorption features derived not only from the presence of oxygen vacancies but also from $2E_g \rightarrow 2T_{2g}$ transitions from O to Cu atoms and d–d transitions from copper ions. TiO_2 nanosheets samples containing a 6 mol% of Cu displayed the best catalytic results, achieving a NH_3 production rate of 78.9 μmol g^{-1} h^{-1} and quantum yields in the range of 0.05–0.25% when using different monochromatic lights from 700 to 400 nm (Fig. 4B and C). Additional photocurrent and time-resolved photoluminescence (PL) decay measurements together with DFT calculations demonstrated that doped TiO_2 nanosheets exhibited an improved charge separation of electron–hole pairs owing to the presence of VO acting as electron-trapping sites.

In a related precedent, Tang and collaborators reported the synthesis of porous carbon-doped anatase TiO_x (C–TiO_x) nanosheets obtained from the thermal-oxidation etching of Ti_3SiC_2.[66] As a result of the carbon doping, the obtained C-TiO_x material displayed a high concentration of Ti^{3+} species that could be easily adjusted by modifying the synthetic conditions. According to both steady-state and time-resolved PL analysis, authors found that the Ti^{3+} sites could act as electron traps to extend the lifetime of charge carriers, compared to the un-doped TiO_2. N_2 chemisorption measurements also indicated that C–TiO_x samples exhibited a high amount of active sites for N_2 activation. All these features, together with an extended light absorption in the visible region thanks to the carbon doping, contributed to the enhancement of the catalytic activity of C–TiO_x nanosheets towards the photo-catalytic N_2 reduction. At the optimal Ti^{3+} concentration, the as-prepared material showed a remarkable NH_3 production of 109.3 μmol g^{-1} h^{-1} under visible light and an apparent quantum efficiency of 1.1% at 400 nm. All these results suggest that the introduction of both oxygen vacancies and/or Ti^{3+} sites is a powerful strategy to improve the efficiency of TiO_2-based catalysts for photo-catalytic N_2 reduction.

Besides defect engineering, surface functionalization represents an alternative route to enhance the catalytic activity of TiO_2-based photo-catalysts. Traditionally, noble metals like platinum, palladium or ruthenium have been proposed as potential co-catalysts in combination with TiO_2. However, the rise of plasmonic photo-chemistry has recently shifted the attention to alternative metals like Au or Ag that present intense plasmon bands in the visible-NIR range. Apart from the extended light absorption, the creation of a metal/semi-

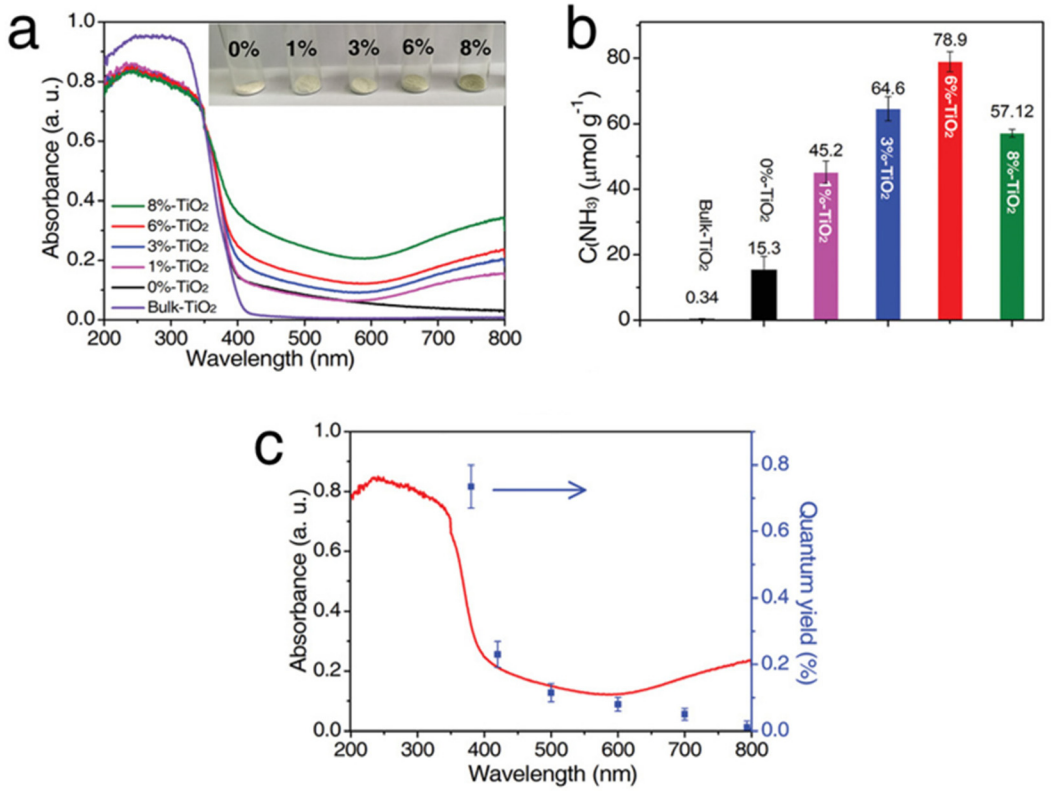

Fig. 4 (a) UV-vis diffuse reflectance spectra (DRS) of TiO_2 nanosheets with different percentages of Cu doping. (b) NH_3 yield of different TiO_2 nanosheets samples under UV-vis radiation (c) UV-vis diffuse reflectance spectrum and quantum efficiency for NH_3 evolution by 6%-TiO_2 sample under monochromatic light of different wavelengths. Reproduced with permission from ref. 65. Copyright (2019) John Wiley and Sons.

conductor heterojunction favors the formation of a Schottky barrier that facilitates the injection of plasmon-induced energetic electrons from the metal to the semiconductor and, at the same time, prevents the return of those electrons back to the metal, thereby improving the charge separation at the heterojunction interface. An appealing example of this approach can be found in the work of Yang and collaborators, where they describe the decoration of oxygen vacancy-containing TiO_2 nanosheets with Au nanocrystals (Au/TiO_2-OV) and its application in the N_2 photo-reduction reaction.[67] Authors claimed a tandem pathway for the N_2 reduction by Au/TiO_2-OV catalyst, where both oxygen vacancies and Au nanocrystals contributed to improve the catalytic performance. In fact, the catalytic activity increased not only with the number of oxygen vacancies in the TiO_2 but also with the loading of Au, achieving a NH_3 production rate close to 100 μmol $g^{-1}h^{-1}$ using a 2.53 wt% Au. It is worth mentioning that authors employed a 420 nm cut-off filter during the experiments, so the catalytic performance entirely derived from the excitation of Au nanocrystals. Indeed, the analysis of the action spectrum revealed a clear match with the absorption spectrum of Au/TiO_2-OV, therefore indicating that the photo-induced hot electrons from plasmonic Au crystals were responsible for the N_2 reduction. Mechanistic studies including N_2 chemisorption, transient absorption spectroscopy (TAS) and photo-voltage measurements suggested that, on the one hand, oxygen vacancies acted as active sites for the activation of N_2 molecules while; on the other hand, Au nanoparticles provided plasmon-induced hot electrons to drive the photo-reduction towards NH_3.

Feng *et al.* also explored the functionalization of oxygen vacancy-enriched TiO_{2-x} with plasmonic Ag nanoparticles and $PW_{10}V_2$ to create a ternary composite for N_2 photo-reduction.[68] In this case, a Z-scheme heterojunction between TiO_2 and $PW_{10}V_2$ was responsible of the N_2 reduction, where electrons and holes were located at the TiO_2 conduction band (CB) and $PW_{10}V_2$ valence band (VB), respectively. Upon plasmon excitation, Ag nanoparticles injected hot electrons to the CB of TiO_2, thus improving the charge separation and increasing the number of available electrons for the N_2 reduction, as demonstrated by transient photo-current and PL measurements. For a broader analysis on the state-of-the-art for the photo-catalytic N_2 reduction reaction by plasmonic structures, readers are referred to an excellent review from Puertolas and collaborators.[56]

Bi-based catalysts. A pioneer work from Zhang and collaborators in which authors demonstrated the photo-reduction of N_2 using BiOBr nanosheets set the basis for a broad field of study on Bi-based photo-catalysts.[69] Since then, different strategies have been adopted in order to improve the catalytic performance of Bi-based catalysts such as defect engineering, surface functionalization or the assembly of heterostructures, among others.[70]

For example, Di *et al.* prepared Bi_3O_4Br layers with surface-confined defects based on Bi and O vacancies.[71] Authors found a clear positive relationship between the degree of defects of the Bi_3O_4Br materials and the amount of NH_3 generated under light radiation. Both femtosecond transient absorption spectroscopy (fs-TAS) and time-resolved transient PL measurements indicated that the presence of defects was responsible of an enhancement in the charge carrier separation owing to the capacity of defects to act as electron traps. In spite of these encouraging results, a serious weakness of this work relies on the catalytic stability tests, which were limited to only 4 consecutive cycles. Unfortunately, this reduced number of catalytic cycles is insufficient to properly assess the stability of the catalyst under study. Xu and collaborators induced defects on pristine bismuth subcarbonate ($Bi_2O_2CO_3$) through hydrothermal treatment of $NaBiO_3$ with graphitic carbon nitride.[72] Importantly, authors found that the introduction of defect levels improved the light absorption properties of the samples, showing and extended absorption towards the NIR region. Consequently, defective $Bi_2O_2CO_3$ displayed catalytic activity towards NH_3 production under visible light, in sharp contrast with the pristine counterpart. It is worth mentioning that the defect density also determined the position of the defect level, so there was an optimum degree of defects to maximize the catalytic performance.

An alternative approach for the formulation of new Bi-based photo-catalysts is the design of heterojunctions combining two or more elements. The group of Wang recently reported the synthesis of a Bi_2MoO_6/BiOBr composite containing both bismuth and oxygen vacancies.[73] Interestingly, bismuth vacancies not only modulated the band position of the composite but also induced the formation of additional oxygen vacancies. The synergy between bismuth and oxygen vacancies led to an improvement in the light absorption properties of the resulting heterostructure. Furthermore, bismuth vacancies provided adequate adsorption sites for N_2 activation. As a result, the composite displayed a ~4-fold NH_3 production compared to the samples with a poor content of defects. Stability tests were performed for 5 consecutive cycles, showing a slightly decrease in the catalytic performance that authors attributed to the partial loss of oxygen vacancies under reaction conditions. The same group expanded this approach through the design of a ternary heterostructure, namely a Bi@BiOBr-Bi_2MoO_6 composite fabricated by two consecutive solvothermal methods.[74] Both semiconductors, BiOBr and Bi_2MoO_6, created a type-II heterojunction in which, under light radiation, photo-excited electrons migrated to the CB of Bi_2MoO_6 and holes accumulated at the VB of BiOBr. Owing to the surface plasmon resonance of metallic Bi and the presence of oxygen vacancies derived from the solvothermal treatments, the light absorption properties of the composite extended towards the IR region of the spectrum. All in all, the combination of the three elements had a positive effect on the catalytic performance, achieving a NH_3 photo-reduction rate as high as 167.2 μmol g^{-1} h^{-1}. In this regard, other Bi-based ternary heterojunctions containing plasmonic particles have been proposed, for instance a combination of graphitic carbon nitride, Bi particles and Bi_2WO_6 to create a g-C_3N_4@Bi@Bi_2WO_6 composite or a heterostructure made of

TiO_2, Au particles and (TiO_2/Au/BiO_4I).[75,76] Furthermore, besides classical semiconductors other potential candidates to fabricate heterojunctions with Bi-based materials have recently included MOFs, MXenes or even graphenes.[77–79]

Other semiconductor-based catalysts

In addition to TiO_2 and Bi-based catalysts, other families of semiconductors have drawn the attention of researchers as promising candidates to drive the photo-catalytic reduction of N_2. For instance, niobates are a well-known class of materials that have been extensively explored as catalysts for photo-catalytic H_2 evolution and, in the last years, they have shown a great potential for the N_2 photo-fixation.[80,81] In 2019, the groups of Zhao and He described a Ag/$KNbO_3$ nanocomposite prepared by a hydrothermal method followed by photo-deposition of Ag nanoparticles.[82] Authors found that it was possible to modulate the morphology, crystallinity and textural properties of $KNbO_3$ by adjusting both the amount of KOH and the hydrothermal temperature during the material synthesis. Under optimal conditions, $KNbO_3$ nanorods decorated with a 0.5% Ag molar ratio displayed a remarkable NH_3 production rate of 385 μmol L^{-1} g_{cat}^{-1} h^{-1} under simulated sunlight using ethanol as hole scavenger. Given the wide bandgap of $KNbO_3$, the photo-activity under visible light was exclusively attributed to Ag nanoparticles, which injected plasmon-induced hot electrons to the CB of $KNbO_3$ to drive the N_2 reduction to NH_3. In a follow-up work from the same group, authors tried to substitute the precious Ag nanoparticles by a more affordable co-catalyst. Hence, authors photo-deposited NiO nanoparticles on $KNbO_3$ and the as-prepared NiO/$KNbO_3$ composite reached a NH_3 productivity as high as 470 μmol L^{-1} g_{cat}^{-1} h^{-1} under simulated sunlight.[83] In this case, both NiO and $KNbO_3$ semiconductors formed a type-II heterojunction that favored charge migration across the heterostructure, with electrons and holes concentrating at the CB of $KNbO_3$ and VB of NiO, respectively.

Metal sulphides are also a long-established family of materials for photo-catalytic applications. With respect to N_2 photo-fixation, a pioneer work from Miyama and collaborators in 1980 proposed for the first time the use of Pt-CdS as photo-catalyst for NH_3 production.[84] Since then, different examples of sulphide-based photo-catalysts for N_2 fixation have been reported.[85–88] One of the main advantages of metal sulphides is their low bandgap that allows for the exploitation of low-energy wavelengths in the visible range (λ > 400 nm).[89] However, metal sulphides usually suffer from low stability and fast charge carrier recombination, thus hampering their broad applicability.[90–92] These drawbacks have motivated intense lines of research to improve the stability and charge separation efficiency of metal sulphides. One of these strategies consists in the fabrication of heterojunctions between metal sulphides and other semiconductors. For instance, in 2020 Sun *et al.* prepared CdS nanorods functionalized with sulfur vacancy-rich 1T MoS_2 nanosheets (SV-1T-MoS_2).[93] The as-prepared SV-1T-MoS_2/CdS composite with optimal MoS_2 loading (30%) showed a photo-catalytic NH_3 production of 8221 μmol L^{-1} g_{cat}^{-1} h^{-1} with an AQE of 4.4% using methanol as sacrificial agent. This value represented a ~4-fold enhancement compared to bare CdS, thus evidencing the positive effect of MoS_2 nanosheets as co-catalyst. In this case, the introduction of MoS_2 containing sulfur vacancies improved the electron mobility and charge carrier separation, as demonstrated by both steady-state and time-resolved PL, transient photo-current and electrochemical impedance spectroscopy (EIS) measurements (Fig. 5).

DFT studies also revealed that the presence of both MoS_2 and sulfur vacancies was critical to promote N_2 adsorption. In spite of this, the study on the stability of the SV-1T-MoS_2/CdS composite was limited to only three consecutive uses, showing a remarkable 20% decrease compared to the fresh sample. This highlights again the importance of performing longer stability tests to demonstrate the reusability of the photo-catalysts under study, especially on those affected by photo-corrosion events. In a related precedent, the group of Yang fabricated nanoporous films of a WS_2@TiO_2 type II heterojunction.[94] Compared to bare TiO_2, the presence of WS_2 improved the charge carrier separation and transfer, as demonstrated by both the increase in the fluorescence time and the reduced semicircle in the Nyquist plots. Upon optimal WS_2 loading, the WS_2@TiO_2 photo-catalyst rendered a maximum NH_3 production rate of 1390 μmol g_{cat}^{-1} h^{-1} in the absence of any sign of deactivation after 4 consecutive cycles. The proposed reaction mechanism involved the charge carrier generation at WS_2 and subsequent electron transfer to the CB of TiO_2, where they were finally injected into anti-bonding orbitals of N_2. Photo-generated holes were accumulated at the VB of WS_2 and then consumed by the hole scavenger. Other composites including In_2O_3/In_2S_3 microspheres, MoS_2/n-$MgIn_2S_4$ sheets or g-C_3N_4/ZnMoCdS have been also reported although in all these cases the catalytic performance was far from adequate.[95–97]

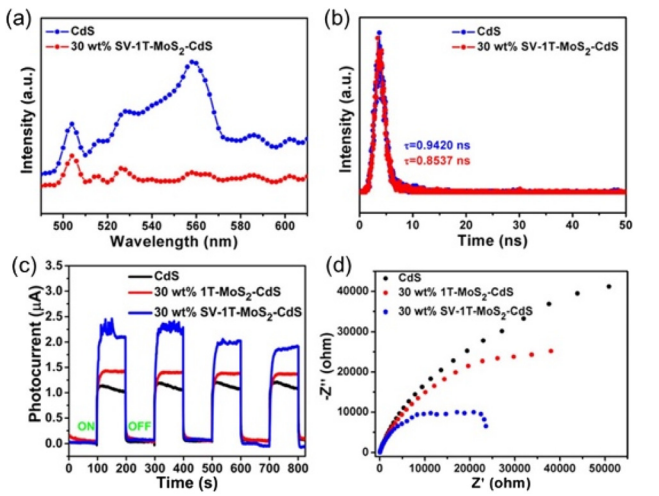

Fig. 5 (a) Steady state and (b) time-resolved PL spectra of CdS nanorods and 30 wt% SV-1T-MoS_2/CdS composites at λ_{ex} = 405 nm. (c) Transient photo-current measurements and (d) EIS Nyquist plots of CdS nanorods, 30 wt% SV-1T-MoS_2/CdS and 30 wt% 1T-MoS_2/CdS composites. Reproduced with permission from ref. 93. Copyright (2020) American Chemical Society.

In addition to the above-discussed semiconductor-based photo-catalysts, the use of tungsten oxides has recently sparked the interest of the scientific community. Although pristine WO_3 has shown a slight activity towards the N_2 photo-reduction, the doping with Fe (0.25%) increased by 4 times the productivity up to 477 μg $gcat^{-1}$ h^{-1} thanks to the improved charge mobility and charge separation efficiency.[98] As for the case of TiO_2-based catalysts, the introduction of oxygen vacancies or dopants to tungsten oxides is a straightforward method to enhance their catalytic activity. In 2022, Yang and collaborators compared the catalytic activity of both 2D WO_{3-x} nanosheets and WO_{3-x} nanoparticles containing a high and low content of oxygen vacancies, respectively.[99] The introduction of oxygen vacancies in the tungsten oxide lattice featured a series of advantages including extended light absorption, improved charge carrier separation and enhanced N_2 adsorption. Consequently, 2D WO_{3-x} nanosheets with abundant oxygen vacancies displayed a NH_3 production of 82.41 μmol g_{cat}^{-1} h^{-1} under irradiation with a visible LED (λ = 420 nm), which was almost 4 times higher compared to the sample with a low content of oxygen vacancies. The stability tests, however, were limited to only 5 cycles and authors did not provide any explanation to the observed deactivation of the catalyst upon consecutive uses. Zhang *et al.* studied the effect of Mo doping on the photo-catalytic activity of $W_{18}O_{49}$ nanowires and it was found that the Mo–W centers acted as active sites for N_2 activation thanks to the polarization of chemisorbed nitrogen molecules.[100] Consequently, Mo-doped $W_{18}O_{49}$ nanowires displayed a 7-fold higher NH_3 production compared to pristine $W_{18}O_{49}$, thus achieving 195 μmol NH_3 g_{cat}^{-1} h^{-1}. In a related precedent, Zhang and co-workers demonstrated that oxygen vacancies displayed a dual effect to both induce the hydrogen spillover and promote N_2 adsorption on Ru-decorated $W_{18}O_{49}$.[101] Under irradiation, photo-generated electrons migrated to Ru NPs to activate and dissociate H_2O in the form of H* while oxygen vacancies facilitated the migration of the H* species to $W_{18}O_{49}$. Eventually, H* species reacted with adsorbed N_2 to produce NH_3. Recycling experiments showed, however, that the catalyst lost its activity upon consecutive reuses. Interestingly, apart from tungsten, other oxides from the same group like molybdenum ones have been investigated as active materials for N_2 photo-fixation. Thanks to the presence of oxygen vacancies, defective molybdenum oxides featured plasmonic behavior that provided extended light absorption along the visible and NIR regions, thus exhibiting remarkable catalytic activities for N_2 photo-reduction.[102,103] More recently in 2023, Fu *et al.* also described the use of defective ZrO_{2-x} in combination with Ru NPs to create a metal/semiconductor heterojunction.[104] In this case, the presence of oxygen vacancies in the zirconia lattice induced a higher concentration of carriers, therefore providing more electrons for the N_2 reduction reaction. Furthermore, the formation of a Schottky barrier at the interface between the defective ZrO_{2-x} and the Ru NPs improved the charge separation and the effective injection of electrons from the semiconductor to the metal.

Carbon-based materials

In addition to inorganic semiconductors, metal-free carbon-based materials have attracted a great deal of attention as affordable and sustainable candidates for applications in catalysis, especially when these materials are obtained from biomass or other renewable sources.[105] In this regard, graphitic carbon nitride (g-C_3N_4) is one of the most relevant examples of this family of materials and its applications span from heterogeneous organic synthesis to photo- and electrocatalysis, among others.[106,107] When it comes to N_2 photo-fixation, a cutting-edge work of 2015 from Dong and co-workers demonstrated for the first time that g-C_3N_4 containing nitrogen vacancies could perform the photo-reduction of N_2 gas under visible light.[108] Not surprisingly, the study demonstrated that nitrogen vacancies are crucial to endow g-C_3N_4 with the capability to photo-reduce N_2 thanks to the improved nitrogen adsorption and enhanced charge transfer efficiency.

Apart from the introduction of vacancies, doping with heteroatoms is a straightforward approach to expand the light absorption properties and modulate the redox potentials of g-C_3N_4.[109] In 2020, Liang and collaborators explored the possibility to merge the positive effects of both nitrogen vacancies and boron-doping in a graphitic carbon nitride.[110] With that purpose, authors first obtained a defective carbon nitride (CN_x) through calcination of melamine followed by an annealing treatment under N_2 in presence of $NaBH_4$ (Fig. 6A). The as-prepared boron-doped defective carbon nitride ($BNUCN_x$) displayed a remarkable NH_3 production rate of 435 μmol g^{-1} h^{-1} under visible light. Both steady-state PL and EIS spectra and photo-current measurements revealed that the defective boron-doped carbon nitride featured a good charge separation efficiency and a low charge-transfer resistance that ultimately improved the catalytic activity (Fig. 6B and C). Furthermore,

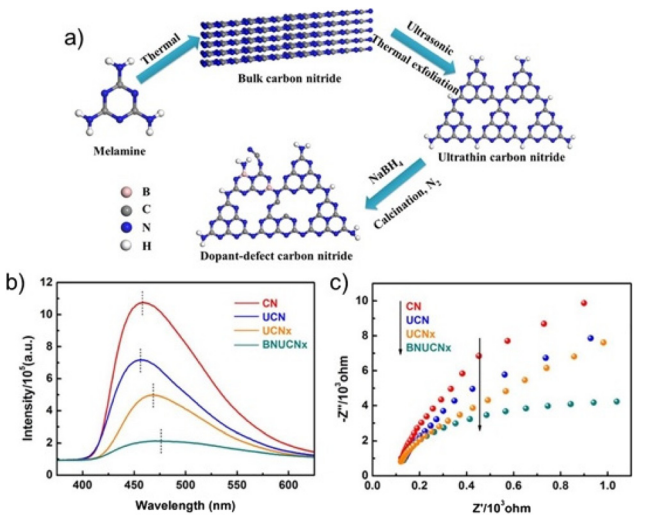

Fig. 6 (a) Schematic illustration of the synthesis protocol for the preparation of boron-doped defective ultrathin carbon nitride ($BNUCN_x$). (b) Steady state PL and (c) EIS spectra of different samples. Reproduced with permission from ref. 110. Copyright (2020) Elsevier.

the introduction of N vacancies and B dopants led to a narrowing in the bandgap that enhanced the optical absorption properties of the final material. In the same spirit, other researchers have investigated the effect of the doping of g-C_3N_4 with diverse heteroatoms such as S or P.[111,112]

As in the case of inorganic semiconductors, the construction of heterojunctions containing g-C_3N_4 can be a useful tool to refine its electronic and catalytic properties. Among all of the different types of heterojunctions, type-II heterojunctions are one of the most investigated systems. For instance, the groups of Zhang and Wu studied the combination of p-type Cu_2O and n-type C_3N_4 semiconductors to build a composite for N_2 photo-fixation.[113] The strong electric field at the interface between both elements greatly enhanced the charge separation efficiency, with electrons and holes accumulating at g-C_3N_4 and Cu_2O, respectively. Another example of type-II heterojunction between g-C_3N_4 and ZrO_2 was reported recently by Mou *et al.*[114] Upon light radiation, photo-excited electrons migrated from the CB of g-C_3N_4 to the CB of ZrO_2, remaining the holes at g-C_3N_4. Thanks to the effective charge separation, the g-C_3N_4/ZrO_2 heterostructure displayed a NH_3 production rate as high as 1446 μmol L^{-1} h^{-1}, compared to the negligible activity of both elements separately. Apart from type-II heterojunctions, Z-scheme heterojunctions are also a very representative exponent of composite materials with improved catalytic efficiencies. In spite that Z-scheme heterostructures feature a distinct design compared to type-II heterojunctions, both architectures provide a spatial separation of electron and holes and the creation of well-defined redox active sites.[115] Several examples of Z-scheme heterostructures for N_2 photo-reduction include g-C_3N_4/Fe_2O_3, g-C_3N_4/Ga_2O_3 or B-doped g-C_3N_4/WO_3.[116–118] For a more comprehensive revision on g-C_3N_4-based materials and heterostructures for photo-catalytic N_2 reduction, readers are referred to excellent reviews covering this topic.[115,119]

Although g-C_3N_4 has been, by far, the most widely explored metal-free material, other carbon-based materials such as doped graphenes, reduced graphene oxides or carbon nanotubes have been investigated, alone or in the form of heterostructures, as potential photo-catalysts for NH_3 production.[120–124] It is worth reminding that, especially for N containing photo-catalysts such as g-C_3N_4 or N-doped carbons, the incorporation of a set of control experiments including the use of isotopically labelled $^{15}N_2$, blank experiments working under N_2-free atmosphere and/or in the absence of photo-catalyst is crucial to ensure the reliability of the reported results. Despite it is out of the scope of the present review, readers will find excellent guidelines for the accurate evaluation of the catalytic activity in N_2 photo-fixation experiments elsewhere.[125–127]

Metal–organic frameworks (MOFs)

In addition to commonly studied inorganic semiconductors and carbon-based materials, metal–organic frameworks are a novel class of materials that can be effectively used as photocatalysts due to their tunability, wide light harvesting properties and large surface area. Applications include photocatalytic water splitting, CO_2 reduction and organic photosynthesis, among others.[128–130] Unfortunately, the study of metal–organic frameworks as photo-catalysts for ammonia synthesis is still in its initial stage.

To date, the greatest number of publications is devoted to transition metal-based metal–organic frameworks. Quite remarkable NH_3 production rates were achieved using iron-based MOFs.[131] In the case of MIL-101(Fe), MIL-88(Fe) and MIL-100 (Fe), the ammonia yield reached 1007.1 μmol g^{-1} h^{-1}, 800.7 μmol g^{-1} h^{-1} and 930.64 μmol g^{-1} h^{-1}, respectively (Fig. 7). The difference between isoreticular iron-based and chromium-based MIL-101, which exhibited no activity, was explored in the same study. Lower activation energy and higher electron density due to two additional filled d-orbitals were identified as fundamental reasons for such a different behavior.

However, Min Luo *et al.* showed that the incorporation of silver particles into the MIL-101(Cr) cavity allowed reaching an activity of 138.81 μmol NH_3 g^{-1} h^{-1}, which they attributed to the synergy of ligand–metal charge transfer (LMCT) and localized surface plasmon resonance effect (LSPR).[132] Inspired by naturally occurring multi-metal cluster nitrogenases, Zhao *et al.* recently synthesized MIL-53(Fe^{2+}/Fe^{3+}), which displayed high nitrogen fixation activity as high as 306 μmol NH_3 g^{-1} h^{-1}.[133] It is important to note that the sample was irradiated only in the visible range above 420 nm, which means that it can potentially be used to convert solar energy. In a similar vein, Li and co-workers adopted a strategy to mimic the functionality of natural enzymes in synthetic materials.[134] In this case, the approach involved modifying the MIL-88A iron MOF with polyoxometalates, which acted as charge regulators and simulated the π*-back-donating mechanism of nitrogenase. This modification resulted in a remarkable six-fold increase in the photocatalytic activity of the MOF.

Some Ti-based MOFs have been explored in photocatalytic reactions and have shown good nitrogen sorption capacity, thus standing for potential catalysts in the N_2 photo-fixation reaction. Huang *et al.* showed that a decrease in the optical band gap of NH_2-MIL-125(Ti) led to an increase in the photo-

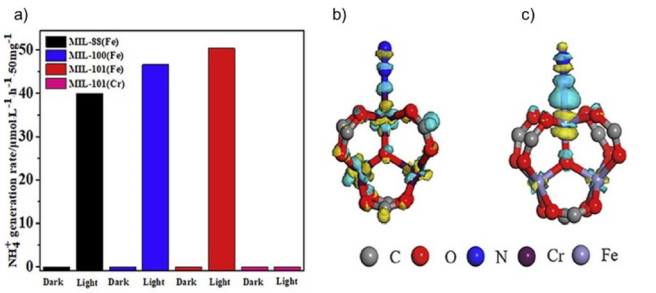

Fig. 7 (a) Photo-catalytic nitrogen fixation activity of different MIL MOFs. Charge density difference of a N_2 molecule adsorbed at (b) MIL-101(Cr) and (c) MIL-101(Fe). Reproduced with permission from ref. 131. Copyright (2020) Elsevier.

catalytic performance, as in the case of hydrogen evolution reaction.[135] However, this Ti-MOF, which exhibits one of the most impressive H_2 evolution activities, reached a very modest NH_3 production of 12.3 μmol g^{-1} h^{-1}. It should be mentioned, however, that the photocatalytic nitrogen reduction tests were tested under visible light and without a sacrificial agent. Interestingly, hafnium and zirconium-containing MOFs (UiO-66-Vis and U(0.5 Hf)) turned out to be ten times more active (256.6 μmol NH_3 g^{-1} h^{-1} and 351 μmol NH_3 g^{-1} h^{-1}, respectively).[136,137] In fact, a recent work indicated that Zr-based MOFs activity could be increased *via* the incorporation of Ca^{2+} dopants, resulting in a noteworthy increase in photocatalytic activity from 105 μmol g^{-1} h^{-1} in the unmodified MOF to 222.2 μmol g^{-1} h^{-1} in the modified counterpart.[138] Authors suggested that the introduction of Ca^{2+} dopants promoted the redistribution of electrons around active Zr sites, thus reducing the activation energy of N_2 triple bonds as elucidated through DFT calculations. Furthermore, the utilization of porphyrins and metalloporphyrins as ligands for stable Zr-based MOF represents an alternative approach to formulate new photocatalysts for NH_3 production.[139] Hence, using porphyrin ligands for MOF construction led to NH_3 production rates of 776.24 μmol g^{-1} h^{-1}, while replacing the ligands with metalloporphyrin resulted in a significant boost in photocatalytic activity, reaching 1502.51 μmol g^{-1} h^{-1}.

Besides transition metal-based, attention should be paid to lanthanide-based MOFs since Hu *et al.* developed two radical-containing gadolinium-based MOFs.[140] Purple crystals of Gd-IHEP-7 could be obtained using a solvothermal technique. The procedure for obtaining Gd-IHEP-8 included heating Gd-IHEP-7 to 120 °C in the air when single-crystal-to-single-crystal transformation occurred. The rearrangement of the Gd^{3+} coordination environment was accompanied by an increase in photocatalytic nitrogen fixation activity (up to 220 μmol NH_3 g^{-1} h^{-1}). Authors suggested that the factor responsible for the higher activity of Gd-IHEP-7 was the calculated change in the stability of the intermediates. Interestingly, Gd-IHEP-7 and Gd-IHEP-8, unlike most other viologen-based compounds, were stable in air and water due to radical–radical interaction. Compared to Gd-based MOFs, deficient activity (34.2 μmol NH_3 g^{-1} h^{-1}) was shown in the case of cerium-based MOF-76 (Ce) even using full-spectrum light of Xe-lamp.[141]

Photo-thermal catalytic NH_3 synthesis

As we have earlier discussed in this review, the thermo-catalytic NH_3 synthesis route is constrained by its harsh operative conditions whereas the photo-catalytic NH_3 production is extremely hampered by its poor catalytic efficiency and low selectivity. In order to overcome these limitations, a smart approach would be the combination of these two strategies into a single process. In this spirit, photo-thermal catalysis arises from the synergistic incorporation of thermal and non-thermal contributions of light and features exceptional advantages compared by its individual counterparts. In fact, this cooperative effect has implications in both reaction thermodynamics and kinetics. For instance, from the thermodynamic point of view, non-thermal effects can reduce the energetic barriers of certain reaction steps. The reduction in the activation energy can derive from charge transfer events to the surface of the catalyst that alter the acidity/basicity of the active sites. Besides, the energy transfer to certain vibrational modes of the transition state can also favour bond elongation, thus decreasing the energy requirements of the process.[142] In this regard, Song and collaborators recently demonstrated the potential of non-thermal effects to adjust the thermodynamics of dry reforming reaction.[143] Authors demonstrated that photo-induced hot electrons from plasmonic Pt and Au nanoparticles could be injected to adsorbed CO_2 and CH_4 molecules, thereby weakening the C═O and C–H bonds and facilitating bond dissociation. In this case, the apparent activation energy under radiation decreased from 241 to 171 kJ mol^{-1}, suggesting a change in the energetics of the reaction. In addition to this, the presence of non-thermal effects opens up the possibility to activate specific chemical bonds that unlock certain reaction pathways that are inaccessible under pure thermal conditions, thus facilitating tailored selectivity patterns or alternative low-energy reaction intermediates. For instance, the groups of Liu and Everitt demonstrated that it was possible to adjust product selectivity in the photo-thermal CO_2 hydrogenation by plasmonic Rh nanoparticles.[144] The use of blue or UV LEDs to perform the reaction facilitated the CH_4 production with selectivities up to 98%, while the reaction under dark conditions displayed comparable amounts of CH_4 and CO. Theoretical calculations demonstrated that the injection of photo-induced hot electrons from Rh nanoparticles to anti-bonding orbitals of adsorbed intermediates played a crucial role to determine the selectivity patterns. Curiously, the presence of hot carriers can not only tune the reaction selectivity towards the desired products, but also prevent the formation of detrimental surface species. Indeed, several recent studies have shown the hot carriers' potential in mitigating the formation of unwanted byproducts, especially in the context of photo-thermal dry reforming of methane.[145,146]

When it comes to thermal effects, the photo-induced heat at the nanoscale provides high temperatures at the active sites in a more efficient way compared to traditional thermo-catalysis. These elevated temperatures translate into catalytic activities that are several orders of magnitude above those obtained with conventional photo-catalysis, mainly due to both the improved reaction kinetics and energy-mass transfer. In addition to this, thermal effects favor the desorption of products or poisonous species from the catalyst surface, thereby enhancing the activity and stability of the catalysts.[147] Last but not least, while in photo-catalytic systems the use of light is limited by the band gap and the position of both conduction and valence bands of the photocatalysts, photo-thermal catalysis takes advantage of the full solar spectrum, even the low-energy photons from the visible and IR that are typically unable to trigger photo-chemical reactions. A comprehensive discussion on the fundamentals of photo-thermal catalysis

and the benefits from the synergies underlying the photo-thermal phenomenon lies beyond the scope of this review, so readers are referred to specific works on this topic.[148–151]

Photo-thermal catalysis can be considered a relatively recent sub-field of catalysis and, in fact, only a few research groups have explored the combination of light and heat to perform the HB process under mild reaction conditions. For instance, García and co-workers lately reported the use of Cs-promoted ruthenium NPs supported on strontium titanate (Cs_yRu_x@ST) as photo-catalyst for the NH_3 synthesis reaction under 350 °C and ambient pressure.[152] All the tests were performed using a continuous-flow set up equipped with a heating ribbon and a thermocouple to control the temperature. Under optimal Cs and Ru loading, the photo-catalyst achieved an impressive NH_3 production rate in the order of 3.6 mmol g^{-1} h^{-1}, outperforming by a 68% a control experiment in the dark at the same temperature. Authors suggested that the remarkable catalytic activity derived from the combination of both photo-induced hot carrier and local thermal effect mechanisms taking place at the irradiated Ru NPs. Altogether, both contributions facilitated the activation of N_2 and its further hydrogenation (Fig. 8A). Interestingly, this work also showed that the choice of the support for Ru NPs was not trivial at all, as authors demonstrated that both the basicity and low thermal conductivity of strontium titanate were key to improve the catalytic performance (Fig. 8B). In 2023, the same group explored the MOF-derived approach to obtain Cs-promoted Ru clusters supported on ZrO_2 as photocatalyst for the photo-thermal NH_3 synthesis.[153] In this case, the authors impregnated the UiO-66 MOF with Ru and Cs precursors and calcined the resulting material in air at 550 °C. Under these conditions, the MOF served as sacrificial template to obtain ZrO_2 decorated with Cs and Ru clusters. The as-obtained catalyst exhibited a notable activity under 350 °C and 1 sun radiation, achieving a NH_3 production rate of 5.1 mmol g^{-1} h^{-1}. Analogous materials prepared by impregnation of commercial ZrO_2 displayed negligible catalytic activity, thus stressing the potential of the MOF-derived strategy to formulate efficient catalysts that are not achievable by conventional synthetic routes. Mechanistic experiments revealed that both thermal and non-thermal effects operated simultaneously to enhance the catalytic activity. On the one hand, Ru sites absorbed visible and NIR light and locally increased the temperature of the catalyst owing to plasmon excitation. On the other hand, plasmon excitation could also generate hot electrons that could be injected into anti-bonding orbitals of adsorbed N_2.

Nevertheless, for most of the photo-thermal systems, it is still extremely challenging to provide an accurate evaluation of the specific role of each of the contributions to the overall catalytic activity. Zhang and collaborators recently addressed this issue employing a model catalyst based on Ru on carbon.[154] Authors first estimated a local temperature of the catalyst ($T_{reaction}$) based on the thermodynamic equilibrium conversion. By introducing this $T_{reaction}$ into the Arrhenius equation under thermo-catalytic conditions, authors calculated the actual reaction rate derived from pure thermal effects ($R_{temperature}$). Once the thermal component was isolated, it was possible to extract the non-thermal contribution ($R_{electron}$) by subtracting the thermal component to the total photo-thermal rate (R_{PTC}). Interestingly, authors found that $R_{electron}$ transitioned from a linear to superlinear relationship with the light intensity, thus confirming the presence of non-thermal effects in the system. In fact, under 5.3 W cm^{-2} light intensity and 350 °C the hot-electron contribution accounted for a 73.6% of the total NH_3 production rate. *In situ* diffuse reflectance infrared Fourier transform spectroscopy (DRIFTS) measurements also revealed the presence of $*NH_x$ species under light radiation at 230 °C, while no intermediates were detected under dark conditions at temperatures below 260 °C. Based on these observations and additional DFT calculations, authors concluded that light could promote the NH_3 synthesis reaction at lower temperatures thanks to the injection of photo-induced hot-electrons into unoccupied anti-bonding orbitals of adsorbed N_2, thus facilitating the cleavage of the N≡N triple bond. Overall, this study demonstrated that it is possible to differentiate and quantify both the thermal and non-thermal contributions of photo-thermal systems using Le Chatelier's principle to determine the actual reaction temperature.

As commented before, local heat generation at the nanoscale is considered one of the main advantages of photo-

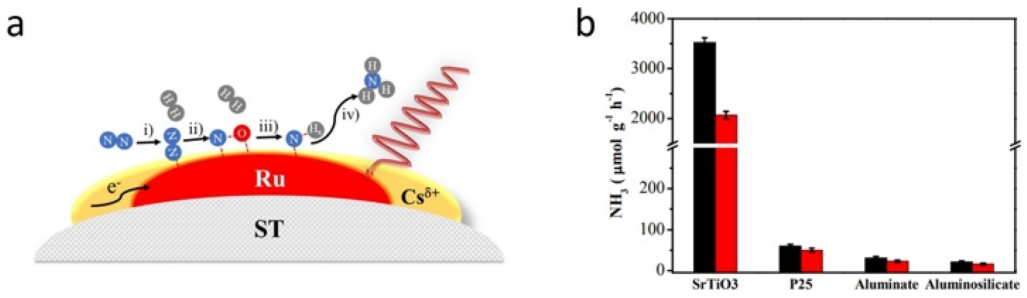

Fig. 8 (a) Proposed mechanism for the photo-thermal NH_3 synthesis by Cs_yRu_x@ST catalyst: (i) N_2 adsorption and activation, (ii) N_2 dissociation and formation of intermediate species, (iii) hydrogenation of activated nitrogen species, and (iv) NH_3 formation and desorption. (b) NH_3 production rate using different supports. Dark bars correspond to experiments under light irradiation and red bars correspond to dark conditions. Reproduced with permission from ref. 152. Copyright (2022) American Chemical Society.

thermal catalysis. In 2019, Mao and co-workers proposed a dual-temperature-zone catalyst to tentatively trick the thermodynamic equilibrium limit while using sunlight to promote the NH_3 synthesis.[155] The idea here was to locate the N_2 dissociation in a "local high-temperature" center, where the nitrogen dissociation takes place, and a local low-temperature center for the N-hydrogenation in order to physically separate these two elemental steps of ammonia synthesis. Thanks to the afore-mentioned capability of photo-thermal catalysis to create hot spots, authors succeeded in designing a catalytic system to provide this non-uniform heat distribution, something otherwise extremely complex to achieve under pure thermal conditions. In this case, plasmonic Fe nanostructures acted as nano-heaters to perform the N_2 dissociation step while subsequent N–H hydrogenation took place at the "cooler" surface of defective $TiO_{2-x}H_y$ owing to its low thermal conductivity. When irradiated at 102 sun, the catalyst reached a temperature as high as 495 °C, thus achieving a NH_3 concentration of 1939 ppm. This concentration was above the thermodynamic equilibrium value of NH_3 synthesis at 495 °C and 1 atm (1249 ppm) and even outperformed the value obtained by commercial-wüstite-based Fe catalyst. The presence of the dual-temperature-zone between Fe and $TiO_{2-x}H_y$ was key to allocate the elementary steps of NH_3 synthesis into two spatially separated catalytic sites, thus surpassing the thermodynamic limit of the reaction (Fig. 9).

Despite the potential of the aforementioned dual-temperature-zone catalyst, some authors have called the attention to the existence of important thermal gradients due to the shallow penetration of light, especially in the case of thick catalyst beds. This situation would, inevitably, confine the effect of photo-thermal catalysis to the illuminated surface region. In their work of 2019, Li *et al.* made the most of this light-induced thermal gradient to boost the NH_3 production rate using a conventional cesium-promoted Ru on magnesium oxide (Cs–Ru/MgO) catalyst.[156] Authors demonstrated that the non-isothermal gradient between the surface and the bottom of the catalyst bed favored high temperatures on the surface, where the N_2 scission took place, while the cooler temperatures from the bottom preserved the NH_3 yield. In addition to this, authors found that not only the presence but also the sign of the thermal gradient was critical to enhance the catalytic activity. Under a negative gradient, thermophoretic forces place parallel to the flow of reactants, thus removing NH_3 products from the hottest region and circumventing the undesirable reverse reaction of NH_3 decomposition. However, under the same absolute value, a positive gradient displayed much lower reaction rates and product yields. Overall, these results evidenced the potential of light-induced thermal gradients to act as thermodynamic pumps to shift the equilibrium and improve the catalytic activity of photo-thermal systems (Fig. 10).

An appealing example of the potential of photo-thermal catalysis to unlock new reaction pathways was reported in 2018 by the group of Zhang. In their work, authors described the use of K-promoted Ru NPs supported on disordered $TiO_{2-x}H_x$ (K/Ru/$TiO_{2-x}H_x$) as photo-thermal catalyst for the solar-driven NH_3 synthesis.[157] The K/Ru/$TiO_{2-x}H_x$ catalyst featured a series of advantages that have been described along previous sections of this review such as the introduction of oxygen vacancies to expand the light absorption properties of TiO_2 or the use of alkaline promoters to tune the electronic environment of Ru NPs and promote N_2 activation. However, the most striking observation in this work was the presence of two simultaneous reaction mechanisms within the K/Ru/$TiO_{2-x}H_x$ catalyst. Hence, activated N_2 could react not only with H atoms on the Ru surface, but also with the H atoms incorporated in the $TiO_{2-x}H_x$ support. Remarkably, this latter pathway was notably different from those reported to date and it could even occur under room temperature, thus suggesting a mechanism

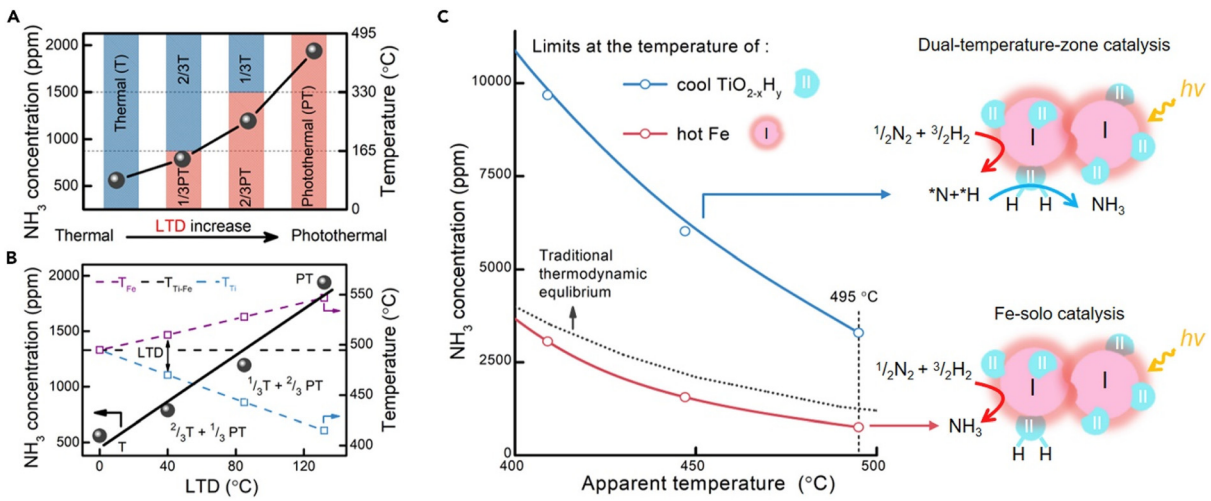

Fig. 9 (A) NH_3 concentration under combined solar irradiation and external heating by $TiO_{2-x}H_y$/Fe at a constant temperature of 495 °C. (B) NH_3 concentration as a function of the local temperature difference (LTD). (C) Comparison of equilibrium limits at the temperature of "cool" $TiO_{2-x}H_y$ and "hot" Fe for photo-thermal ammonia synthesis on $TiO_{2-x}H_y$/Fe (1 atm). Reproduced with permission from ref. 155. Copyright (2019) Elsevier.

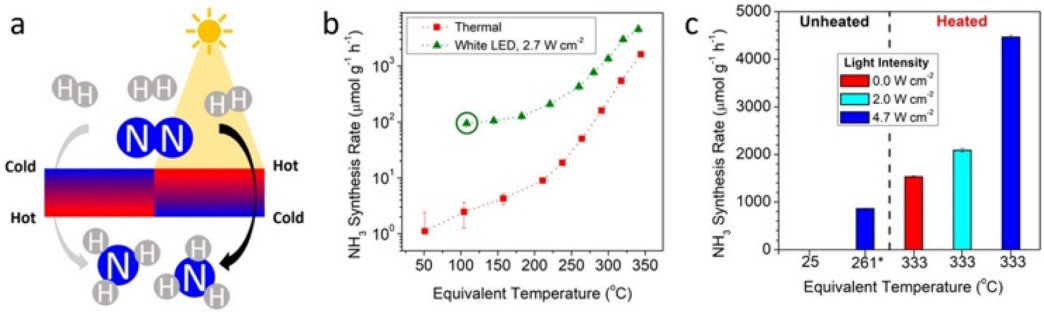

Fig. 10 (a) Illustration of the thermal gradient generated by the photo-thermal heating of the irradiated catalyst surface. Effect of light-induced thermal gradients on NH_3 synthesis. (b) Measured dark thermal (red squares) and heated white light illumination NH_3 synthesis rates as a function of equivalent temperature. Circled data point indicates the light-only condition with no external heating applied. (c) NH_3 synthesis rates under dark and additionally illuminated conditions using a blue LED. Reproduced with permission from ref. 156. Copyright (2019) American Chemical Society.

with a considerably low energy barrier. In fact, authors calculated the activation energies of both thermal and photo-thermal reactions, achieving 86 and 65 kJ mol^{-1}, respectively. This decrease in the activation energy was explained by the presence of both plasmon-induced confined magnetic fields and heat generation at the vicinity of Ru NPs. In general, this study opened a new venue for the development of alternative NH_3 synthesis routes driven by solar light thanks to the combination of low-energy reaction pathways and the confined energy of plasmonic NPs.

Catalyst engineering and optimization

As mentioned before, photo-thermal catalysts benefit from a synergistic contribution of both photo and thermal components of light. To further intensify the photo-thermal effect and enhance production rates, researchers have focused on improving the light-to-heat conversion by optimizing size and shape of active sites, adjusting the porosity and nature of support or through structural engineering, among other strategies.[148]

For plasmonic materials, size and shape of nanoparticles affect not only the capability of charge carrier generation, but also the thermal properties.[158] Theoretical calculations indicate that smaller nanoparticles produce electron–hole pairs with higher energy in comparison to larger nanoparticles.[159] This characteristic holds significant importance in the context of photo-thermal catalysis, as it enhances the likelihood of populating acceptor states and overcoming Schottky barriers. However, a small particle size may lead to inefficient charge carrier separation due to spatial confinement. In addition, larger particles also show a red-shift on the absorption capability of the catalyst, unlocking the use of visible and IR light ranges.[160] Another point is that the plasmon-heating effect in metallic nanoparticles scales quadratically with their radius.[161] Therefore, the engineering of the ideal catalyst relies on the perfect balance of the size. As for the morphology, geometries that display strong and inhomogeneous electric fields associated with confinement effects contribute to high-energy hot electrons and holes.[162] The opposite is also true, geometries without defects and homogeneous electric fields, like nanospheres, exhibit a less efficient production of hot carriers.

Another possibility is to use secondary light-absorbing elements, whereby a catalytically active metal is coupled with another material able to absorb light in a wider range and generate photo-carriers and/or heat.[163–165] Core–shell structures have also received great attention, as the idea is to mimic a nanoreactor, confining the heat in the core, increasing the temperature precisely where the active sites are located.[166] Still in this context, MOFs can also be used as sacrificial templates to obtain carbon-based materials featuring broadband light absorption in the visible and IR light ranges.[11] The combination of carbonaceous supports with highly dispersed metal nanoparticles makes MOF-derived materials a very attractive family of catalysts for photo-thermal applications.[167]

Conclusions and outlook

Due to its widespread use as building block for the production of fertilizers, NH_3 is considered one of the key chemicals in our society. Despite the technological maturity of the Haber–Bosch process, there is still room for improvement. With this objective in mind, ongoing research is being devoted not only to find catalysts able to operate under milder conditions without losing productivity, but also to the development of alternative synthetic routes. One of the possibilities in this regard is the integration of light into the NH_3 synthesis process to achieve photo-catalytic N_2 fixation routes powered by sunlight. However, to date the reported efficiencies remain far from those required to compete with the conventional HB approach. In an effort to overcome the limitations of both thermo- and photo-catalytic approaches, photo-thermal catalysis has demonstrated potential to achieve high activities at moderate reaction conditions through the synergistic combination of thermal and non-thermal contributions of sunlight.

In this review, we have first provided an overview of the main reaction pathways for NH_3 synthesis. Next, we have reviewed recent strategies for the formulation of novel catalysts for the thermo-catalytic NH_3 production able to operate at

milder conditions. In this regard, catalysts based on Ru or Co are considered promising candidates although their higher costs compared to inexpensive Fe-based catalysts still represent a major pitfall for their wide implementation. Later, we have discussed potential methodologies to improve the catalytic performance of photo-catalytic systems for N_2 photo-fixation, mainly the introduction of vacancies, defects or the construction of heterojunctions. In the last section of the review, we highlighted the significance of photo-thermal catalysis to surpass the limitations of its individual counterparts thanks to the synergistic integration of thermal and non-thermal effects. This cooperative effect can improve reaction rates, create positive thermal gradients or even trigger alternative lower-energy reaction pathways.

Although the technological advantages are evident, to date there has been little discussion on the benefits of photo-thermal catalysis in terms of sustainability. A rigorous analysis in this regard would require appropriate metrics to evaluate the environmental impact of photo-thermal catalysis but, unfortunately, these figures of merit have not been perfectly established in the field. Ozin and collaborators recently tried to address this issue and proposed a series of equations to assess the CO_2 footprint of thermal and photo-thermal CO_2 hydrogenation reactions.[168] These equations considered multiple parameters related to the photo-thermal process such as CO_2 emissions per kWh of electricity, CO_2 produced per mol of H_2, total irradiation time or the power consumption of lamps, pumps, *etc*., among others. Based on their model, authors found that the source of radiation was critical to reduce the CO_2 emissions associated with the photo-thermal process. In other words, energy-saving lamps with low power are preferred, as the net CO_2 emission rate scales up with the power of the lamp. In the best-case scenario, the direct use of sunlight instead of electricity would further reduce the carbon footprint or even achieve negative CO_2 emissions, although this strategy would require additional technological development. Equations also indicated that reactor configuration plays an important role, as flow reactors displayed a higher potential to reduce CO_2 emissions compared to their batch counterparts. Assuming a CO_2-free source of H_2, authors concluded that photo-thermal catalysis has the potential to achieve net CO_2 emission rates lower than traditional thermal catalysis, especially in the case of flow reactors coupled with energy-efficient lamps or directly powered with solar radiation. Overall, this pioneer work reinforced the prospects of the photo-thermal approach in terms of its CO_2 footprint and set the basis for subsequent studies focused on other chemistries of interest beyond CO_2 hydrogenation. In addition to this, assessing the economic feasibility of the entire process is imperative to ensure a realistic scale-up of this technology. While performing an accurate economic analysis of the photo-thermal HB process is highly challenging due to the immaturity of the field and the lack of actual data from large-scale prototypes, we would like to share some considerations for future estimations. Based on available techno-economic analyses, the main contributors to the total energy consumption in blue ammonia production include the ammonia separation refrigerant, cooling water and gas used to provide heat to the reactors.[6] In the case of green ammonia, electricity for compressors, water for general cooling and refrigerant for separation purposes are the major contributors to the energy requirements of the operation. With this in mind, the photo-thermal approach could potentially reduce the energy demand (and consequently, the cost) of the process by harnessing natural sunlight instead of relying on electricity or gas to power the HB reactors. Furthermore, considering that photo-thermal processes can operate at lower temperatures than pure thermal systems, the energy costs could be further reduced. The techno-economic analysis should also include the cost of the photo-thermal reactor based on parameters such as the average solar intensity, illumination hours, irradiated area, type of solar collector, amount and lifetime of the photo-catalyst, *etc*. Nevertheless, previous works have revealed that the major capital costs for NH_3 synthesis primarily stem from feed costs rather than energy costs. This implies that, ultimately, the hydrogen or gas market prices will play a pivotal role to determine the profitability of any potential route for NH_3 production.[6]

Despite its promising future, if photo-thermal catalysis is to lead a paradigm shift in the field of heterogeneous catalysis and compete with long-established thermo-catalytic processes, a series of challenges need to be addressed. For instance, a deeper understanding of the synergies between hot carriers and thermal effects at the fundamental level would be desirable in order to fully comprehend the mechanisms underlying photo-thermal reactions. To this end, *in situ*/*in operando* techniques (X-ray diffraction, electron microscopy, XPS, Fourier-transformed IR, Raman, UV-vis absorption, *etc*.…) could help not only to assess the contribution of thermal and non-thermal effects on the catalytic performance, but also to provide full information on the catalytic sites and transitional species present under reaction conditions.[169–172] In this regard, computational methods can be also interesting tools to disentangle not only the reaction pathways but also the intermediate states involved.

An accurate measurement of the local temperature is crucial in photo-thermal catalysis as imprecise temperature records can lead to misinterpretations of the thermal contribution.[173] For this reason, and especially in the case of thick catalyst beds, one or more sets of thermocouples should be utilized to ensure a correct monitoring of the temperature across the catalyst. Ideally, these measurements should be complemented with additional temperature registrations using IR cameras or temperature-responsive photoluminescence probes.

From the point of view of scalability, photo-thermal catalysis requires adequate photo-reactors capable of harvesting sunlight and channeling it directly to the catalyst. Based on lessons learned from a mature technology like the solar thermal energy, solar concentrators or condenser lenses could serve as elements to both harness and concentrate sunlight.[174–176] For instance, the groups of Steinfeld and

Furler recently developed a solar fuel system that enables the production of syngas from water and CO_2 using concentrated solar energy.[177] The solar redox unit consisted of a sun-tracking parabolic concentrator coupled with a secondary reflector. Under normal solar radiation conditions, the system could reach a peak flux concentration above 5000 suns and an average flux of approximately 2700 suns. Many reaction systems, however, require less severe solar flux concentrations in the order of 50 to 100 suns. In these cases, the use of parabolic troughs to reflect and concentrate sunlight can be a more affordable and practical option. These systems use sets of concave mirrors to concentrate light into its focal line, achieving temperatures in the range of 500–700 K.[178] Alternatively, high-power LEDs or incandescent light bulbs could also act as irradiation sources in conjunction or not with solar light radiation.[179] In addition to that, further considerations on heat management should be taken into account when designing new photo-reactors, as thermal management has proved to be critical if one wants to maximize the benefits of the photo-thermal effect. Moreover, the use of batch reactors at the laboratory scale should be progressively shifted to continuous-flow reactors that are better suited for potentially scalable systems at the industrial scale. In any case, it is necessary to perform extensive research in reactor design and engineering to piece together all these considerations and develop suitable photo-reactors for applications in photo-thermal catalysis.

As we have discussed in detail along this review, the HB process is one of the best examples of energy integration in the chemical industry. In this particular case, for photo-thermal catalysis to be successful, catalysts with excellent light absorption and light-to-heat conversion properties are crucial. Examples of this kind of materials include carbon-based solids, defective semiconductors or transition metal carbides and nitrides. These materials, alone or in combination with adequate metallic active sites, can provide exceptional electronic and thermal effects to synergistically boost the production of NH_3 from N_2 and H_2. Along with absorption properties, stability is equally important when assessing the potential application of a catalyst. Conventional stability cycles usually cover only a few hours of activity, however, this limited timespan is insufficient to gain any insight on the real robustness of the system, so long-term stability tests in the order of tens of hours are imperative.

The present review has described alternative NH_3 synthesis routes based on the use of solar light as source of energy, namely photo-catalysis and photo-thermal catalysis. However, it is worth reminding that the use of electro-catalysis to drive the N_2 reduction reaction has recently gained considerable interest. Compared to the traditional HB process, the possibility to produce NH_3 using renewable electricity would allow a decentralized route for N_2 fixation with lower CO_2 emissions and improved energy efficiency. However, in spite of these promising features, the viability and reliability of most of the available reports on electrocatalytic N_2 reduction is still under debate, given the low amount of NH_3 produced (in the orders of nmol to μmol) and the presence of multiple impurities that may lead to false positives.[180–182] For instance, a recent work from Chen and collaborators demonstrated the presence of nitrogen-containing compounds such as NO_3^- or NO_2^- in many commercial catalysts for ammonia electro-synthesis, thus stressing the necessity to develop specific protocols to ensure reliable and reproducible results.[183] In any case, electrochemical NH_3 synthesis has become a very dynamic field of research and we certainly believe it will play a decisive role in the future NH_3 production systems beyond the HB process. For these reasons, and despite being out of the scope of this work, those readers interested in the topic are referred to specific reviews available in the literature.[181,184,185]

In summary, photo-thermal catalysis has proved to hold great promise as a viable route to drive the N_2 hydrogenation to NH_3 using solar light as energy source. Apart from its advantages in terms of energy efficiency and operational costs, a potential niche for the photo-thermal NH_3 synthesis would be the distributed production of fertilizers. Conventional HB facilities tend to be localized close to the natural gas supply points and require daily productions in the range of thousands of metric tons of NH_3 to be economically feasible.[186] These facts illustrate some of the constraints of the HB process, particularly the heavy dependence on fossil fuels and a certain inflexibility in the scale.[4] On the contrary, photo-thermal NH_3 synthesis represents an opportunity for the deployment of small-scale delocalized NH_3 plants powered by renewable energy. This on-site production of ammonia would increase the access to fertilizers, especially in remote or isolated areas, promoting their economic and social growth. Interestingly, besides the well-known application of NH_3 as precursor for the manufacture of fertilizers, in recent years NH_3 has been considered as an excellent H_2 carrier owing to its high volumetric and gravimetric energy density and well-established distribution infrastructure.[187] Nevertheless, the decomposition of NH_3 to obtain N_2 and H_2 is a highly endothermic reaction that requires elevated temperatures in the range of 500–600 °C to achieve significant conversion rates, thus posing a considerable penalty to the overall efficiency. Given its ability to reach elevated local temperatures, photo-thermal catalysis has the potential to drive the light-induced cracking of NH_3 under milder operating conditions, thus lowering the cost and improving the efficiency of the whole process, in a similar way to the NH_3 synthesis reaction. Within the context of hydrogen economy, the development of such a light-mediated NH_3 synthesis-decomposition cycle would be considered a major breakthrough with multiple implications in the decarbonization of a wide variety of areas including transportation or the industrial sector. All in all, we hope that this review will stimulate the progress of new photo-thermal systems focused not only on the chemistry of NH_3 but also on other commodities of industrial interest.

Author contributions

Conceptualization: D.M. and J.G. Writing – original draft: D. M., A.S., M. Z. Writing – review and editing: J.G.

Conflicts of interest

There are no conflicts to declare.

Acknowledgements

Funding from this work was provided by King Abdullah University of Science and Technology (KAUST). Authors would like to thank Mrs Sandra Ramirez for the artwork in this manuscript.

References

1 G. Soloveichik, *Nat. Catal.*, 2019, **2**, 377–380.
2 K. H. Rouwenhorst, Y. Engelmann, K. van't Veer, R. S. Postma, A. Bogaerts and L. Lefferts, *Green Chem.*, 2020, **22**, 6258–6287.
3 L. Wang, M. Xia, H. Wang, K. Huang, C. Qian, C. T. Maravelias and G. A. Ozin, *Joule*, 2018, **2**, 1055–1074.
4 A. J. Martín, T. Shinagawa and J. Pérez-Ramírez, *Chem*, 2019, **5**, 263–283.
5 C. A. Del Pozo and S. Cloete, *Energy Convers. Manage.*, 2022, **255**, 115312.
6 P. Mayer, A. Ramirez, G. Pezzella, B. Winter, S. M. Sarathy, J. Gascon and A. Bardow, *IScience*, 2023, **26**, 107389.
7 **https://www.aramco.com/en/news-media/news/2020/first-blue-ammonia-shipment**, (accessed 14/11/2023).
8 C. Smith, A. K. Hill and L. Torrente-Murciano, *Energy Environ. Sci.*, 2020, **13**, 331–344.
9 X. Xue, R. Chen, C. Yan, P. Zhao, Y. Hu, W. Zhang, S. Yang and Z. Jin, *Nano Res.*, 2019, **12**, 1229–1249.
10 D. Mateo, P. Maity, G. Shterk, O. F. Mohammed and J. Gascon, *ChemSusChem*, 2021, **14**, 5525–5533.
11 I. S. Khan, D. Mateo, G. Shterk, T. Shoinkhorova, D. Poloneeva, L. Garzón-Tovar and J. Gascon, *Angew. Chem.*, 2021, **133**, 26680–26686.
12 S. W. L. Ng, M. Gao, W. Lu, M. Hong and G. W. Ho, *Adv. Funct. Mater.*, 2021, **31**, 2104750.
13 S. Lu, F. Liu, P. Qiu, M. Qiao, Y. Li, Z. Cheng, N. Xue, X. Hou, C. Xu and Y. Xiang, *Chem. Eng. J.*, 2020, **379**, 122382.
14 J. Liao, Y. Xu, Y. Zhao, C.-C. Wang and C. Ge, *ACS Appl. Nano Mater.*, 2021, **4**, 1898–1905.
15 C. Song, Z. Wang, Z. Yin, D. Xiao and D. Ma, *Chem. Catal.*, 2022, **2**, 52–83.
16 H. Shen, M. Yang, L. Hao, J. Wang, J. Strunk and Z. Sun, *Nano Res.*, 2022, 1–37.
17 G. Zhang, Y. Li, C. He, X. Ren, P. Zhang and H. Mi, *Adv. Energy Mater.*, 2021, **11**, 2003294.
18 M. A. Shipman and M. D. Symes, *Catal. Today*, 2017, **286**, 57–68.
19 M. Li, H. Huang, J. Low, C. Gao, R. Long and Y. Xiong, *Small Methods*, 2019, **3**, 1800388.
20 K. H. Rouwenhorst, A. G. Van der Ham and L. Lefferts, *Int. J. Hydrogen Energy*, 2021, **46**, 21566–21579.
21 H. Liu, *Chin. J. Catal.*, 2014, **35**, 1619–1640.
22 N. Morlanés, W. Almaksoud, R. K. Rai, S. Ould-Chikh, M. M. Ali, B. Vidjayacoumar, B. E. Al-Sabban, K. Albahily and J.-M. Basset, *Catal. Sci. Technol.*, 2020, **10**, 844–852.
23 R. K. Rai, W. Al Maksoud, N. Morlanés, M. Harb, R. Ahmad, A. Genovese, M. N. Hedhili, L. Cavallo and J.-M. Basset, *ACS Catal.*, 2021, **12**, 587–599.
24 P. Yan, W. Guo, Z. Liang, W. Meng, Z. Yin, S. Li, M. Li, M. Zhang, J. Yan, D. Xiao, R. Zou and D. Ma, *Nano Res.*, 2019, **12**, 2341–2347.
25 Y. Tang, Y. Kobayashi, N. Masuda, Y. Uchida, H. Okamoto, T. Kageyama, S. Hosokawa, F. Loyer, K. Mitsuhara and K. Yamanaka, *Adv. Energy Mater.*, 2018, **8**, 1801772.
26 M. Kitano, J. Kujirai, K. Ogasawara, S. Matsuishi, T. Tada, H. Abe, Y. Niwa and H. Hosono, *J. Am. Chem. Soc.*, 2019, **141**, 20344–20353.
27 N. Saadatjou, A. Jafari and S. Sahebdelfar, *Chem. Eng. Commun.*, 2015, **202**, 420–448.
28 Z. Wang, J. Lin, R. Wang and K. Wei, *Catal. Commun.*, 2013, **32**, 11–14.
29 N. Shimoda, Y. Kimura, Y. Kobayashi, J. Kubota and S. Satokawa, *Int. J. Hydrogen Energy*, 2017, **42**, 29745–29755.
30 B. C. McClaine and R. J. Davis, *J. Catal.*, 2002, **210**, 387–396.
31 X. Zhang, L. Liu, A. Wu, J. Zhu, R. Si, J. Guo, R. Chen, Q. Jiang, X. Ju and J. Feng, *ACS Catal.*, 2022, **12**, 2178–2190.
32 Y. Ma, G. Lan, W. Fu, Y. Lai, W. Han, H. Tang, H. Liu and Y. Li, *J. Energy Chem.*, 2020, **41**, 79–86.
33 C. Liang, Z. Wei, Q. Xin and C. Li, *Appl. Catal., A*, 2001, **208**, 193–201.
34 Z. Ma, X. Xiong, C. Song, B. Hu and W. Zhang, *RSC Adv.*, 2016, **6**, 51106–51110.
35 M. Carltonbird, S. Eaimsumang, S. Pongstabodee, S. Boonyuen, S. M. Smith and A. Luengnaruemitchai, *Chem. Eng. J.*, 2018, **344**, 545–555.
36 Z. Ma, S. Zhao, X. Pei, X. Xiong and B. Hu, *Catal. Sci. Technol.*, 2017, **7**, 191–199.
37 C. Li, Y. Shi, Z. Zhang, J. Ni, X. Wang, J. Lin, B. Lin and L. Jiang, *J. Energy Chem.*, 2021, **60**, 403–409.
38 J. Feng, L. Liu, X. Ju, Q. Jiang, J. Wang, J. Guo, T. He and P. Chen, *Catal. Sci. Technol.*, 2023, **13**, 4156–4167.
39 Y. Baik, M. Kwen, K. Lee, S. Chi, S. Lee, K. Cho, H. Kim and M. Choi, *J. Am. Chem. Soc.*, 2023, **145**, 11364–11374.
40 X. Zhang, L. Liu, J. Wang, X. Ju, R. Si, J. Feng, J. Guo and P. Chen, *J. Catal.*, 2023, **417**, 382–395.
41 J. Feng, L. Liu, X. Zhang, J. Wang, X. Ju, R. Li, J. Guo, T. He and P. Chen, *Catal. Sci. Technol.*, 2023, **13**, 844–853.
42 L. Li, T. Zhang, J. Cai, H. Cai, J. Ni, B. Lin, J. Lin, X. Wang, L. Zheng and C.-T. Au, *J. Catal.*, 2020, **389**, 218–228.
43 Y. Zhou, X. Peng, T. Zhang, H. Cai, B. Lin, L. Zheng, X. Wang and L. Jiang, *ACS Catal.*, 2022, **12**, 7633–7642.
44 M. Kitano, Y. Inoue, H. Ishikawa, K. Yamagata, T. Nakao, T. Tada, S. Matsuishi, T. Yokoyama, M. Hara and H. Hosono, *Chem. Sci.*, 2016, **7**, 4036–4043.

45 M. Kitano, Y. Inoue, M. Sasase, K. Kishida, Y. Kobayashi, K. Nishiyama, T. Tada, S. Kawamura, T. Yokoyama and M. Hara, *Angew. Chem.*, 2018, **130**, 2678–2682.
46 I. Rossetti, N. Pernicone and L. Forni, *Catal. Today*, 2005, **102**, 219–224.
47 T.-N. Ye, S.-W. Park, Y. Lu, J. Li, M. Sasase, M. Kitano, T. Tada and H. Hosono, *Nature*, 2020, **583**, 391–395.
48 W. Gao, J. Guo, P. Wang, Q. Wang, F. Chang, Q. Pei, W. Zhang, L. Liu and P. Chen, *Nat. Energy*, 2018, **3**, 1067–1075.
49 A. Tarka, M. Zybert, E. Truszkiewicz, B. Mierzwa, L. Kępiński, D. Moszyński and W. Raróg-Pilecka, *ChemCatChem*, 2015, **7**, 2836–2839.
50 B. Lin, Y. Liu, L. Heng, J. Ni, J. Lin and L. Jiang, *Catal. Commun.*, 2017, **101**, 15–19.
51 B. Lin, Y. Liu, L. Heng, J. Ni, J. Lin and L. Jiang, *J. Rare Earths*, 2018, **36**, 703–707.
52 X. Wang, L. Li, T. Zhang, B. Lin, J. Ni, C.-T. Au and L. Jiang, *Chem. Commun.*, 2019, **55**, 474–477.
53 Y. Bicer, I. Dincer, C. Zamfirescu, G. Vezina and F. Raso, *J. Cleaner Prod.*, 2016, **135**, 1379–1395.
54 A. J. Medford and M. C. Hatzell, *ACS Catal.*, 2017, **7**, 2624–2643.
55 S. Chen, D. Liu and T. Peng, *Sol. RRL*, 2021, **5**, 2000487.
56 B. Puértolas, M. Comesaña-Hermo, L. V. Besteiro, M. Vázquez–González and M. A. Correa–Duarte, *Adv. Energy Mater.*, 2022, **12**, 2103909.
57 Y. Shi, Z. Zhao, D. Yang, J. Tan, X. Xin, Y. Liu and Z. Jiang, *Chem. Soc. Rev.*, 2023, **52**, 6938–6956.
58 G. Schrauzer and T. Guth, *J. Am. Chem. Soc.*, 2002, **99**, 7189–7193.
59 V. Augugliaro, A. Lauricella, L. Rizzuti, M. Schiavello and A. Sclafani, *Int. J. Hydrogen Energy*, 1982, **7**, 845–849.
60 J. Soria, J. Conesa, V. Augugliaro, L. Palmisano, M. Schiavello and A. Sclafani, *J. Phys. Chem.*, 1991, **95**, 274–282.
61 N. Rao, S. Dube and P. Natarajan, *Appl. Catal., B*, 1994, **5**, 33–42.
62 W. Zhao, J. Zhang, X. Zhu, M. Zhang, J. Tang, M. Tan and Y. Wang, *Appl. Catal., B*, 2014, **144**, 468–477.
63 D. Maarisetty and S. S. Baral, *J. Mater. Chem. A*, 2020, **8**, 18560–18604.
64 L. Ran, J. Hou, S. Cao, Z. Li, Y. Zhang, Y. Wu, B. Zhang, P. Zhai and L. Sun, *Sol. RRL*, 2020, **4**, 1900487.
65 Y. Zhao, Y. Zhao, R. Shi, B. Wang, G. I. Waterhouse, L. Z. Wu, C. H. Tung and T. Zhang, *Adv. Mater.*, 2019, **31**, 1806482.
66 Q. Han, C. Wu, H. Jiao, R. Xu, Y. Wang, J. Xie, Q. Guo and J. Tang, *Adv. Mater.*, 2021, **33**, 2008180.
67 J. Yang, Y. Guo, R. Jiang, F. Qin, H. Zhang, W. Lu, J. Wang and J. C. Yu, *J. Am. Chem. Soc.*, 2018, **140**, 8497–8508.
68 C. Feng, P. Wu, Q. Li, J. Liu, D. Wang, B. Liu, T. Wang, H. Hu and G. Xue, *New J. Chem.*, 2022, **46**, 1731–1740.
69 H. Li, J. Shang, Z. Ai and L. Zhang, *J. Am. Chem. Soc.*, 2015, **137**, 6393–6399.
70 Y. Huang, N. Zhang, Z. Wu and X. Xie, *J. Mater. Chem. A*, 2020, **8**, 4978–4995.
71 J. Di, J. Xia, M. F. Chisholm, J. Zhong, C. Chen, X. Cao, F. Dong, Z. Chi, H. Chen and Y. X. Weng, *Adv. Mater.*, 2019, **31**, 1807576.
72 C. Xu, P. Qiu, L. Li, H. Chen, F. Jiang and X. Wang, *ACS Appl. Mater. Interfaces*, 2018, **10**, 25321–25328.
73 Y. Zhang, S. Gu, X. Zhou, K. Gao, K. Sun, D. Wu, J. Xia and X. Wang, *Catal. Sci. Technol.*, 2021, **11**, 4783–4792.
74 M. Lan, N. Zheng, X. Dong, X. Ren, J. Wu, H. Ma and X. Zhang, *Sustainable Energy Fuels*, 2021, **5**, 2927–2933.
75 J. Wang, L. Tang, G. Zeng, Y. Liu, Y. Zhou, Y. Deng, J. Wang and B. Peng, *ACS Sustainable Chem. Eng.*, 2017, **5**, 1062–1072.
76 X. Yu, H. Qiu, Z. Wang, B. Wang, Q. Meng, S. Sun, Y. Tang and K. Zhao, *Appl. Surf. Sci.*, 2021, **556**, 149785.
77 J. Liu, R. Li, X. Zu, X. Zhang, Y. Wang, Y. Wang and C. Fan, *Chem. Eng. J.*, 2019, **371**, 796–803.
78 X. Chen, Y. Li, Z. Wu, X. Xu, W. Zhu and X. Gao, *J. Colloid Interface Sci.*, 2021, **602**, 553–562.
79 T. Fei, L. Yu, Z. Liu, Y. Song, F. Xu, Z. Mo, C. Liu, J. Deng, H. Ji and M. Cheng, *J. Colloid Interface Sci.*, 2019, **557**, 498–505.
80 C. Ladasiu, N. Kulischow and R. Marschall, *Catal. Sci. Technol.*, 2022, **12**, 1450–1457.
81 F. Yang, Q. Zhang, L. Zhang, M. Cao, Q. Liu and W.-L. Dai, *Appl. Catal., B*, 2019, **257**, 117901.
82 P. Xing, S. Wu, Y. Chen, P. Chen, X. Hu, H. Lin, L. Zhao and Y. He, *ACS Sustainable Chem. Eng.*, 2019, **7**, 12408–12418.
83 P. Xing, W. Zhang, L. Chen, X. Dai, J. Zhang, L. Zhao and Y. He, *Sustainable Energy Fuels*, 2020, **4**, 1112–1117.
84 H. Miyama, N. Fujii and Y. Nagae, *Chem. Phys. Lett.*, 1980, **74**, 523–524.
85 S. Hu, Y. Li, F. Li, Z. Fan, H. Ma, W. Li and X. Kang, *ACS Sustainable Chem. Eng.*, 2016, **4**, 2269–2278.
86 K. A. Brown, D. F. Harris, M. B. Wilker, A. Rasmussen, N. Khadka, H. Hamby, S. Keable, G. Dukovic, J. W. Peters and L. C. Seefeldt, *Science*, 2016, **352**, 448–450.
87 S. Hu, X. Chen, Q. Li, Y. Zhao and W. Mao, *Catal. Sci. Technol.*, 2016, **6**, 5884–5890.
88 Z. He, Y. Wang, X. Dong, N. Zheng, H. Ma and X. Zhang, *RSC Adv.*, 2019, **9**, 21646–21652.
89 K. Zhang and L. Guo, *Catal. Sci. Technol.*, 2013, **3**, 1672–1690.
90 X. Ning, J. Li, B. Yang, W. Zhen, Z. Li, B. Tian and G. Lu, *Appl. Catal., B*, 2017, **212**, 129–139.
91 T. Di, Q. Xu, W. Ho, H. Tang, Q. Xiang and J. Yu, *ChemCatChem*, 2019, **11**, 1394–1411.
92 M. Lan, Y. Wang, X. Dong, F. Yang, N. Zheng, Y. Wang, H. Ma and X. Zhang, *Appl. Surf. Sci.*, 2022, **591**, 153205.
93 B. Sun, Z. Liang, Y. Qian, X. Xu, Y. Han and J. Tian, *ACS Appl. Mater. Interfaces*, 2020, **12**, 7257–7269.
94 L. Shi, Z. Li, L. Ju, A. Carrasco-Pena, N. Orlovskaya, H. Zhou and Y. Yang, *J. Mater. Chem. A*, 2020, **8**, 1059–1065.

95 H. Xu, Y. Wang, X. Dong, N. Zheng, H. Ma and X. Zhang, *Appl. Catal., B*, 2019, **257**, 117932.
96 G. Swain, S. Sultana and K. Parida, *ACS Sustainable Chem. Eng.*, 2020, **8**, 4848–4862.
97 Q. Zhang, S. Hu, Z. Fan, D. Liu, Y. Zhao, H. Ma and F. Li, *Dalton Trans.*, 2016, **45**, 3497–3505.
98 Y. Shen, J. Shou, L. Chen, W. Han, L. Zhang, Y. Chen, X. Tu, S. Zhang, Q. Sun and Y. Chang, *Appl. Catal., A*, 2022, **643**, 118739.
99 Z. Yang, J. Wang, J. Wang, M. Li, Q. Cheng, Z. Wang, X. Wang, J. Li, Y. Li and G. Zhang, *Langmuir*, 2022, **38**, 1178–1187.
100 N. Zhang, A. Jalil, D. Wu, S. Chen, Y. Liu, C. Gao, W. Ye, Z. Qi, H. Ju and C. Wang, *J. Am. Chem. Soc.*, 2018, **140**, 9434–9443.
101 L. Zhang, R. Li, L. Cui, Z. Sun, L. Guo, X. Zhang, Y. Wang, Y. Wang, Z. Yu and T. Lei, *Chem. Eng. J.*, 2023, **461**, 141892.
102 X. Liu, Y. Luo, C. Ling, Y. Shi, G. Zhan, H. Li, H. Gu, K. Wei, F. Guo and Z. Ai, *Appl. Catal., B*, 2022, **301**, 120766.
103 H. Wu, X. Li, Y. Cheng, Y. Xiao, R. Li, Q. Wu, H. Lin, J. Xu, G. Wang and C. Lin, *J. Mater. Chem. A*, 2020, **8**, 2827–2835.
104 R. Fu, G. Wang, Q. Zhan, L. Zhang and L. Liu, *Green Chem.*, 2023, **25**, 8531–8538.
105 S. Navalon, A. Dhakshinamoorthy, M. Alvaro and H. Garcia, *Chem. Rev.*, 2014, **114**, 6179–6212.
106 Y. Wang, X. Wang and M. Antonietti, *Angew. Chem., Int. Ed.*, 2012, **51**, 68–89.
107 F. K. Kessler, Y. Zheng, D. Schwarz, C. Merschjann, W. Schnick, X. Wang and M. J. Bojdys, *Nat. Rev. Mater.*, 2017, **2**, 1–17.
108 G. Dong, W. Ho and C. Wang, *J. Mater. Chem. A*, 2015, **3**, 23435–23441.
109 G. Liao, Y. Gong, L. Zhang, H. Gao, G.-J. Yang and B. Fang, *Energy Environ. Sci.*, 2019, **12**, 2080–2147.
110 C. Liang, H.-Y. Niu, H. Guo, C.-G. Niu, D.-W. Huang, Y.-Y. Yang, H.-Y. Liu, B.-B. Shao and H.-P. Feng, *Chem. Eng. J.*, 2020, **396**, 125395.
111 Z. Li, G. Gu, S. Hu, X. Zou and G. Wu, *Chin. J. Catal.*, 2019, **40**, 1178–1186.
112 Y. Shiraishi, S. Shiota, Y. Kofuji, M. Hashimoto, K. Chishiro, H. Hirakawa, S. Tanaka, S. Ichikawa and T. Hirai, *ACS Appl. Energy Mater.*, 2018, **1**, 4169–4177.
113 K. Zhang, Z. Ai, M. Huang, D. Shi, Y. Shao, X. Hao, B. Zhang and Y. Wu, *J. Catal.*, 2021, **395**, 273–281.
114 H. Mou, J. Wang, D. Yu, D. Zhang, W. Chen, Y. Wang, D. Wang and T. Mu, *ACS Appl. Mater. Interfaces*, 2019, **11**, 44360–44365.
115 L. Zhang, S. Hou, T. Wang, S. Liu, X. Gao, C. Wang and G. Wang, *Small*, 2022, **18**, 2202252.
116 S. Liu, S. Wang, Y. Jiang, Z. Zhao, G. Jiang and Z. Sun, *Chem. Eng. J.*, 2019, **373**, 572–579.
117 S. Cao, N. Zhou, F. Gao, H. Chen and F. Jiang, *Appl. Catal., B*, 2017, **218**, 600–610.
118 K. Zhang, L. Deng, M. Huang, H. Tu, Z. Kong, Z. Liang, Y. Shao, X. Hao and Y. Wu, *Colloids Surf., A*, 2022, **633**, 127830.
119 C. H. Ng, S. H. Teo, N. Mansir, A. Islam, C. G. Joseph, S. Hayase and Y. H. Taufiq-Yap, *Sustainable Energy Fuels*, 2021, **5**, 4457–4511.
120 L. K. Putri, B.-J. Ng, W.-J. Ong, H. W. Lee, W. S. Chang and S.-P. Chai, *J. Mater. Chem. A*, 2018, **6**, 3181–3194.
121 J. Gu, Y. Yu, X. Fu, H. Chen, F. Jiang and X. Wang, *Appl. Surf. Sci.*, 2021, **555**, 149733.
122 S. Hu, W. Zhang, J. Bai, G. Lu, L. Zhang and G. Wu, *RSC Adv.*, 2016, **6**, 25695–25702.
123 X.-H. Li, W.-L. Chen, H.-Q. Tan, F.-R. Li, J.-P. Li, Y.-G. Li and E.-B. Wang, *ACS Appl. Mater. Interfaces*, 2019, **11**, 37927–37938.
124 M. Lashgari and P. Zeinalkhani, *Nano Energy*, 2018, **48**, 361–368.
125 Y. Zhao, R. Shi, X. Bian, C. Zhou, Y. Zhao, S. Zhang, F. Wu, G. I. Waterhouse, L. Z. Wu and C. H. Tung, *Adv. Sci.*, 2019, **6**, 1802109.
126 Y. Zhao, F. Wu, Y. Miao, C. Zhou, N. Xu, R. Shi, L. Z. Wu, J. Tang and T. Zhang, *Angew. Chem., Int. Ed.*, 2021, **60**, 21728–21731.
127 H. Iriawan, S. Z. Andersen, X. Zhang, B. M. Comer, J. Barrio, P. Chen, A. J. Medford, I. E. Stephens, I. Chorkendorff and Y. Shao-Horn, *Nat. Rev. Methods Primers*, 2021, **1**, 56.
128 Y. Xiao, X. Guo, N. Yang and F. Zhang, *J. Energy Chem.*, 2021, **58**, 508–522.
129 W. Zhan, H. Gao, Y. Yang, X. Li and Q. L. Zhu, *Adv. Energy Sustainability Res.*, 2022, **3**, 2200004.
130 S. Abednatanzi, M. Najafi, P. G. Derakhshandeh and P. Van Der Voort, *Coord. Chem. Rev.*, 2022, **451**, 214259.
131 G. Li, F. Li, J. Liu and C. Fan, *J. Solid State Chem.*, 2020, **285**, 121245.
132 X. Zhang, X. Li, S. Su, M. Tan, G. Liu, Y. Wang and M. Luo, *Catal. Sci. Technol.*, 2023, **13**, 705–713.
133 Z. Zhao, D. Yang, H. Ren, K. An, Y. Chen, Z. Zhou, W. Wang and Z. Jiang, *Chem. Eng. J.*, 2020, **400**, 125929.
134 X.-H. Li, H. Li, S.-L. Jiang, L. Yang, H.-Y. Li, Q.-L. Liu, W. Bai, Q. Zhang, C. Xiao and Y. Xie, *ACS Catal.*, 2023, **13**, 7189–7198.
135 H. Huang, X.-S. Wang, D. Philo, F. Ichihara, H. Song, Y. Li, D. Li, T. Qiu, S. Wang and J. Ye, *Appl. Catal., B*, 2020, **267**, 118686.
136 W. Gao, X. Li, X. Zhang, S. Su, S. Luo, R. Huang, Y. Jing and M. Luo, *Nanoscale*, 2021, **13**, 7801–7809.
137 K. An, H. Ren, D. Yang, Z. Zhao, Y. Gao, Y. Chen, J. Tan, W. Wang and Z. Jiang, *Appl. Catal., B*, 2021, **292**, 120167.
138 J. Tan, H. Ren, Z. Zhao, X. Xin, Y. Shi, D. Yang and Z. Jiang, *Chem. Eng. J.*, 2023, **466**, 143259.
139 B. Bagherpour and S. Dehghanpour, *J. Solid State Chem.*, 2023, **324**, 124079.
140 K. Q. Hu, P. X. Qiu, L. W. Zeng, S. X. Hu, L. Mei, S. W. An, Z. W. Huang, X. H. Kong, J. H. Lan and J. P. Yu, *Angew. Chem., Int. Ed.*, 2020, **59**, 20666–20671.

141 C. Zhang, Y. Xu, C. Lv, X. Zhou, Y. Wang, W. Xing, Q. Meng, Y. Kong and G. Chen, *ACS Appl. Mater. Interfaces*, 2019, **11**, 29917–29923.
142 M. Ghoussoub, M. Xia, P. N. Duchesne, D. Segal and G. Ozin, *Energy Environ. Sci.*, 2019, **12**, 1122–1142.
143 H. Song, X. Meng, T. D. Dao, W. Zhou, H. Liu, L. Shi, H. Zhang, T. Nagao, T. Kako and J. Ye, *ACS Appl. Mater. Interfaces*, 2018, **10**, 408–416.
144 X. Zhang, X. Li, D. Zhang, N. Q. Su, W. Yang, H. O. Everitt and J. Liu, *Nat. Commun.*, 2017, **8**, 14542.
145 J. Zhang, K. Xie, Y. Jiang, M. Li, X. Tan, Y. Yang, X. Zhao, L. Wang, Y. Wang and X. Wang, *ACS Catal.*, 2023, **13**, 10855–10865.
146 S. Wu, Y. Li, Q. Hu, J. Wu and Q. Zhang, *ACS Sustainable Chem. Eng.*, 2021, **9**, 11635–11651.
147 Y. Wu, S. Han, Y. Huang, Y. Shi and B. Zhang, *J. Mater. Chem. A*, 2018, **6**, 18426–18429.
148 D. Mateo, J. L. Cerrillo, S. Durini and J. Gascon, *Chem. Soc. Rev.*, 2021, **50**, 2173–2210.
149 N. Keller, J. Ivanez, J. Highfield and A. M. Ruppert, *Appl. Catal., B*, 2021, **296**, 120320.
150 Z. Wang, Z. Yang, R. Fang, Y. Yan, J. Ran and L. Zhang, *Chem. Eng. J.*, 2022, **429**, 132322.
151 J. Hong, C. Xu, B. Deng, Y. Gao, X. Zhu, X. Zhang and Y. Zhang, *Adv. Sci.*, 2022, **9**, 2103926.
152 Y. Peng, J. Albero, A. Franconetti, P. Concepción and H. García, *ACS Catal.*, 2022, **12**, 4938–4946.
153 Y. Peng, A. Melillo, R. Shi, A. Forneli, A. Franconetti, J. Albero and H. García, *Appl. Catal., B*, 2023, **339**, 123143.
154 X. Bian, Y. Zhao, G. I. Waterhouse, Y. Miao, C. Zhou, L. Z. Wu and T. Zhang, *Angew. Chem.*, 2023, **135**, e202304452.
155 C. Mao, H. Li, H. Gu, J. Wang, Y. Zou, G. Qi, J. Xu, F. Deng, W. Shen and J. Li, *Chem*, 2019, **5**, 2702–2717.
156 X. Li, X. Zhang, H. O. Everitt and J. Liu, *Nano Lett.*, 2019, **19**, 1706–1711.
157 C. Mao, L. Yu, J. Li, J. Zhao and L. Zhang, *Appl. Catal., B*, 2018, **224**, 612–620.
158 W. He, X. Huang, X. Ma and J. Zhang, *J. Opt.*, 2022, **51**, 142–153.
159 A. Manjavacas, J. G. Liu, V. Kulkarni and P. Nordlander, *ACS Nano*, 2014, **8**, 7630–7638.
160 S. Link and M. A. El-Sayed, *Int. Rev. Phys. Chem.*, 2000, **19**, 409–453.
161 A. O. Govorov and H. H. Richardson, *Nano Today*, 2007, **2**, 30–38.
162 J. Grand, B. Auguié and E. C. Le Ru, *Anal. Chem.*, 2019, **91**, 14639–14648.
163 L. Zhou, J. M. P. Martirez, J. Finzel, C. Zhang, D. F. Swearer, S. Tian, H. Robatjazi, M. Lou, L. Dong and L. Henderson, *Nat. Energy*, 2020, **5**, 61–70.
164 Y. Yuan, L. Zhou, H. Robatjazi, J. L. Bao, J. Zhou, A. Bayles, L. Yuan, M. Lou, M. Lou and S. Khatiwada, *Science*, 2022, **378**, 889–893.
165 R. Verma, R. Tyagi, V. K. Voora and V. Polshettiwar, *ACS Catal.*, 2023, **13**, 7395–7406.
166 J. Shen, R. Tang, Z. Wu, X. Wang, M. Chu, M. Cai, C. Zhang, L. Zhang, K. Yin and L. He, *Trans. Tianjin Univ.*, 2022, **28**, 236–244.
167 I. S. Khan, L. Garzon-Tovar, D. Mateo and J. Gascon, *Eur. J. Inorg. Chem.*, 2022, **2022**, e202200316.
168 S. Wang, A. A. Tountas, W. Pan, J. Zhao, L. He, W. Sun, D. Yang and G. A. Ozin, *Small*, 2021, **17**, 2007025.
169 L. Wang, Y. Dong, T. Yan, Z. Hu, A. A. Jelle, D. M. Meira, P. N. Duchesne, J. Y. Y. Loh, C. Qiu and E. E. Storey, *Nat. Commun.*, 2020, **11**, 2432.
170 L. Zhang, Y. Zhang, X. Huang, L. Tao and Y. Bi, *Appl. Catal., B*, 2021, **283**, 119633.
171 T. H. Tan, B. Xie, Y. H. Ng, S. F. B. Abdullah, H. Y. M. Tang, N. Bedford, R. A. Taylor, K.-F. Aguey-Zinsou, R. Amal and J. Scott, *Nat. Catal.*, 2020, **3**, 1034–1043.
172 D. Mateo, J. Albero and H. Garcia, *Joule*, 2019, **3**, 1949–1962.
173 L. Mascaretti, A. Schirato, T. Montini, A. Alabastri, A. Naldoni and P. Fornasiero, *Joule*, 2022, **6**, 1727–1732.
174 M. Romero and A. Steinfeld, *Energy Environ. Sci.*, 2012, **5**, 9234–9245.
175 Y. Tian and C.-Y. Zhao, *Appl. Energy*, 2013, **104**, 538–553.
176 A. A. Khan and M. Tahir, *J. CO2 Util.*, 2019, **29**, 205–239.
177 R. Schäppi, D. Rutz, F. Dähler, A. Muroyama, P. Haueter, J. Lilliestam, A. Patt, P. Furler and A. Steinfeld, *Nature*, 2022, **601**, 63–68.
178 J. Zhang, H. Chen, X. Duan, H. Sun and S. Wang, *Mater. Today*, 2023, **68**, 234–253.
179 X. E. Cao, Y. Kaminer, T. Hong, P. Schein, T. Liu, T. Hanrath and D. Erickson, *Iscience*, 2020, **23**, 101856.
180 L. F. Greenlee, J. N. Renner and S. L. Foster, *Journal*, 2018, **8**, 7820–7827.
181 C. Tang and S.-Z. Qiao, *Chem. Soc. Rev.*, 2019, **48**, 3166–3180.
182 J. Choi, B. H. Suryanto, D. Wang, H.-L. Du, R. Y. Hodgetts, F. M. Ferrero Vallana, D. R. MacFarlane and A. N. Simonov, *Nat. Commun.*, 2020, **11**, 5546.
183 Y. Chen, H. Liu, N. Ha, S. Licht, S. Gu and W. Li, *Nat. Catal.*, 2020, **3**, 1055–1061.
184 H. Shen, C. Choi, J. Masa, X. Li, J. Qiu, Y. Jung and Z. Sun, *Chem*, 2021, **7**, 1708–1754.
185 G. Qing, R. Ghazfar, S. T. Jackowski, F. Habibzadeh, M. M. Ashtiani, C.-P. Chen, M. R. Smith III and T. W. Hamann, *Chem. Rev.*, 2020, **120**, 5437–5516.
186 N. Okuzumi, B. Jones and S. Nielsen, Start-up of the world largest ammonia plant, *Proceedings of NITROGEN*, 2001.
187 N. Morlanés, S. P. Katikaneni, S. N. Paglieri, A. Harale, B. Solami, S. M. Sarathy and J. Gascon, *Chem. Eng. J.*, 2021, **408**, 127310.